An Electronic Model of Neuroelectric Point Processes*

E. R. LEWIS
Department of Electrical Engineering and Computer Sciences and the Electronics Research Laboratory
University of California, Berkeley, California

Received March 18, 1968

Zusammenfassung. Eine umfassende Darstellung der Nervenzellmembran wird durch eine Kombination von Hodgkin-Huxley-Beschreibung der elektrisch erregbaren Leitwerte und Eccles-Beschreibung der synaptisch induzierten Leitwerte wiedergegeben. Diese Darstellung wird in einem elektronischen Modell veranschaulicht. Nichtlineare aktive Schaltungen werden benützt, um Leistungen zu entwickeln, die in ihrer Form mit den zeit- und spannungsabhängigen Leitwerten der Beschreibungen übereinstimmen. Die Leistungen werden mit Hilfe von Multiplikatoren in äquivalente Leitwerte umgewandelt. Das elektrische Modell enthält 24 kontrollierbare Parameter, von denen jeder mit einem in der Beschreibung übereinstimmt. Zur Einstellung der Parameter sollte man eine Strategie benützen, die soweit wie möglich die Werte von HODGKIN und HUXLEY (s. Tafel) als Parameter verwendet. Kleine Abweichungen von diesen Werten werden als mindere Störungen der grundliegenden Zusammenstellung betrachtet. Als Beispiel einer systematischen Untersuchung des Einflusses einer Veränderung verschiedener Parameter wurden die Spannungsschwingungen gewählt. Die Frequenz der ungedämpften Schwingungen beträgt ungefähr 50 Hertz. Verschiedene andere kleine Änderungen der Parameter können Schwingungsfrequenzen von 4 Hertz hervorrufen. Mit großen Störungen der Grundwerte kann man auch Schwingungsfrequenzen im Werte 1 Hertz erlangen.

Es wird vorgeschlagen, daß die kombinierten Eccles- und Hodgkin-Huxley-Beschreibungen die Mehrzahl der neuroelektrischen Vorgänge einzelner Nervenzellen darstellen könnten. Dieser Vorschlag wird durch weitere Ergebnisse bestätigt. Die Beobachtung wird jedoch ausgedrückt, daß die zusammenfassende Darstellung in wenigstens einem Falle, den Nervenzellen des Hummer-Herznervenknotens, nicht zulänglich ist.

I. Introduction

During the past ten years, considerable effort has been spent modeling nerve cells and networks of nerve cells. Normally an introduction should bring the reader up to date on the particular subject being discussed; but 78 journal pages were required recently to review just some of the accomplishments of neural modelers (HARMON and LEWIS, 1966), and a 78 page introduction would lead to all sorts of disagreeable repercussions. May I summarize the work of the past ten years, then, with a few general comments?

Most neural models can be interpreted as representing hypotheses about some aspect of neurophysiology. Often a hypothesis includes complicated interactions of several variables and one cannot easily deduce its consequences. The role of the model is to facilitate deduction, to be the deductively manipulable representative of the hypothesis. Only after its consequences are known, in considerable quantitative detail, can a hypothesis truly be subjected to the kind of scrutiny demanded by good science. The model's role, therefore, is not insignificant.

Several modeling studies have been designed to test hypotheses concerning neuroelectric interactions within a single neuron. Models were used to test the following hypothesis, for example (RALL, 1964): the apparent anomalies of the transient electrical potentials observed in certain neurons are the results of the distributed, passive electrical properties of dendrites. In another instance, it was postulated that the Hodgkin-Huxley descriptions of neuroelectric processes in the squid axon could be extended in simple ways to account for anomolous responses, such as plateau potentials, in that axon. Models were used to test the hypothesis (FITZ HUGH, 1960).

Other modelers have considered a problem potentially much more complex than neuroelectric interactions in one cell; they have considered the possibility of modeling portions of a central nervous system. The tacit hypothesis at the very outset of such considerations is that the details of neuroelectric interactions within individual neurons become progressively less important as one considers larger and larger neural networks. A hypothesis subordinate to this might take the form of a list of those properties of individual neurons that the modeler considers important in neural networks. Many neural models have been accompanied in print by extensive lists of the neuronal properties represented and, occasionally, by extensive lists of those properties missing from other models. It has been pointed out that polemic occasionally replaces science in neural modeling (HARMON, 1964). Length and completeness of a property list are not virtues in themselves. Each new property list is merely a statement of a new hypothesis; and it is quite possible that the longer lists represent hypotheses that are more unwieldy and less amenable to scrutiny than those represented by the shorter lists.

I have not included a property list in this paper, because the models described here were designed for studies of neuroelectric interactions in single cells or in very small groups of cells. These models represent the following hypothesis: the Hodgkin-Huxley descriptions of electrically excitable conductances can be combined with the Eccles descriptions of synaptically induced conductances to account for most of the neuroelectric phenomena exhibited by single neurons. To the extent that this hypothesis is correct, it provides a basis for highly detailed modeling of neural networks. Unfortunately, however, the Hodgkin-Huxley and Eccles descriptions are very complicated — involving conductances that depend on time or voltage or both. A quick glance at the circuit diagrams in this paper will reveal how ridiculous a network study with these models could be.

The important questions of neurophysiology are not totally related to large, central structures, however; many important questions concern very small groups of neurons, groups in which details of neuroelectric phenomena may be very important. The models described in this paper were designed for studies of such groups. Already they have been used to simulate

* Research sponsored by the Joint Services Electronics Programm under Grant AF-AFOSR-139-67, the Librascope Group, General Precision Systems, Inc., Glendale, California, under Air Force Office of Scientific Research USAF Contract No. AF 49(638)-1232, and by the 6570th Aerospace Medical Research Laboratories, Air Force Systems Command, USAF Cotract No. AF 33(615)-2464.

possible neuroelectric interactions among regions of a single neuron and interactions between two neurons with various interconnections (LEWIS, 1968a, b). In addition, they have been used in a simulation study of the nine-neuron lobster cardiac ganglion (LEWIS, 1968b). The models themselves are essentially two-terminal networks. One terminal represents the inside of a nerve-cell membrane; the other terminal represents the outside. Between these two terminals are seven electrical circuits in parallel, each representing an equivalent shunt admittance across the nerve cell membrane (see Fig. 1). The four elements on the right of the dashed line in Fig. 1 represent the four shunt admittances of the Hodgkin-Huxley model of the membrane of the squid giant axon (HODGKIN and HUXLEY, 1952d). The three elements on the left of the dashed line represent the three synaptic admittances postulated by ECCLES and others (ECCLES, 1964). The complete network illustrated in Fig. 1 is a point model, because it represents neuroelectric phenomena at a single point in space (i.e., on a patch of membrane, over which voltages do not vary with distance). It can represent a small patch of electrically excitable membrane with a contiguous patch of subsynaptic membrane and negligible electrical impedance between the two; or it can represent a larger patch of membrane [e.g., the entire cell body (soma) of a neuron] if transit times for potentials traveling over that patch are negligible compared to the times required for changes in the voltage- and time-dependent admittances across the patch.

A. The Hodgkin-Huxley Model of Squid-Axon Membrane. HODGKIN and HUXLEY inserted a pair of electrodes into the giant axon of the squid and, using one electrode to supply current and the other to monitor voltage, observed the current required to force the potential across an isolated patch of the axon membrane to change in a stepwise manner (HODGKIN et al., 1952). Varying the ionic constituents of the fluid surrounding the axon, they resolved the current into four components: capacitive current, sodium-ion current, potassium-ion current, and leakage current (presumed to be carried by other ions). By defining the driving force behind each ionic current as the difference between the actual potential across the membrane and the potential at which the particular current reversed direction, HODGKIN and HUXLEY (1952d) reduced their data to the equivalent circuit shown on the right of the dashed line in Fig. 1. Their data indicated that the equivalent conductance (G_L) for leakage current and the membrane capacitance (C_M) were constant, but that the equivalent conductances for potassium-ion current (G_K) and sodium-ion current (G_{Na}) were dependent on membrane potential and time. HODGKIN and HUXLEY described the potassium and sodium conductances by means of state variables obeying differential equations with voltage-dependent parameters:

$$G_K = \overline{g_K} n^4 (V_K - V_M),$$

$$\frac{dn}{dt} = \alpha_n (1 - n) - \beta_n n; \quad 0 \leqq n \leqq 1,$$

$$G_{Na} = \overline{g_{Na}} m^3 h (V_{Na} - V_M),$$

$$\frac{dm}{dt} = \alpha_m (1 - m) - \beta_m m; \quad 0 \leqq m \leqq 1,$$

$$\frac{dh}{dt} = \alpha_h (1 - h) - \beta_h n; \quad 0 \leqq h \leqq 1$$

where $\overline{g_K}$ and $\overline{g_{Na}}$ are constants; n, m, and h are state variables; V_K and V_{Na} are the respective potentials at which the potassium current and the sodium current reverse directions; α_n, β_n, α_m, β_m, α_h and β_h are parameters that depend on voltage but not time.

B. The Eccles Model of Subsynaptic Membrane. It has been established that many if not almost all nerve cells communicate with one another by means of chemical synapses. It has been postulated by ECCLES (1964) and others that a spike, reaching the termination of one nerve cell on another, induces emission of a chemical transmitter substance into the extracellular space between the two cells. This transmitter substance apparently induces an increase in one or more

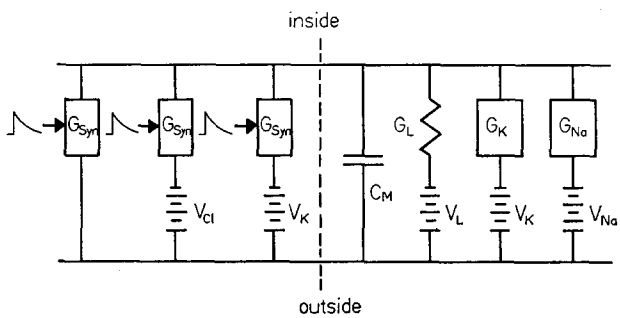

Fig. 1. Circuit equivalent of the combined Eccles, Hodgkin-Huxley descriptions. The elements on the left of the dashed line represent the synaptically induced conductances described by ECCLES (1964). Those on the right of the dashed line represent the elements of excitable membrane, as described by HODGKIN and HUXLEY (1952d)

ionic permeabilities in the subsynaptic membrane of the receiving cell. ECCLES has described these permeability changes in terms of equivalent electrical conductances. It is assumed generally that the equivalent synaptic conductance is directly proportional to the concentration of transmitter present in the space between the sending cell and the receiving cell. This concentration rises abruptly during a presynaptic spike, then falls again toward zero as the transmitter is dissipated or inactivated. If the transmitter is dissipated by a simple diffusion process or inactivated by a first-order chemical process, its concentration following a spike will decay exponentially with time. The synaptically induced equivalent conductances thus will have the forms of decaying exponentials. The current associated with excitatory synapses goes to zero when the potential across the membrane is nearly zero; so the equivalent conductance associated with these synapses apparently is a nonspecific shunt to all ions. Inhibitory synapses, on the other hand, appear to be associated specifically with potassium ions or chloride ions or both. Some inhibitory synapses operate by means of a transient increase of the equivalent potassium conductance, others by a transient increase of the equivalent chloride conductance, and others by means of a combination of chloride and potassium conductances.

C. Methods of Simulation. Since HODGKIN and HUXLEY have provided a reasonably concise mathematical description of the electrical properties of the

squid axon, and since it is quite simple to express mathematically an exponentially decaying conductance, one might be tempted to combine the Hodgkin-Huxley and Eccles descriptions into a single set of simultaneous differential equations. Writing the equations is not at all difficult; solving them would be extremely difficult. The equations are nonlinear and have voltage-dependent coefficients (the Hodgkin-Huxley rate constants) and time-dependent coefficients (the synaptic conductances). These difficulties are amplified fantastically when one considers the equations modified to include spatial variations of neuroelectric phenomena. Rather than analyzing the combined Hodgkin-Huxley-Eccles descriptions by solving nonlinear differential equations, we have chosen to analyze them by constructing electronic realizations of the descriptions and observing the results on a cathode ray oscilloscope.

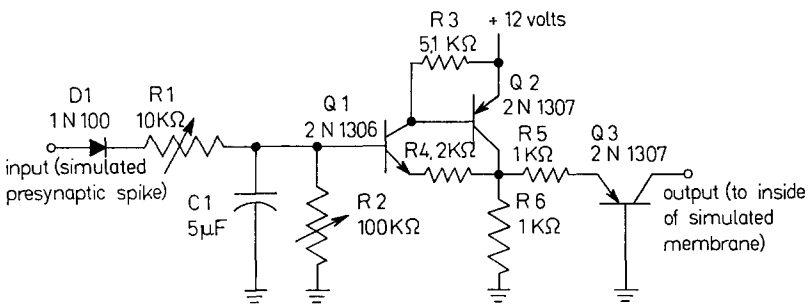

Fig. 2. An electronic circuit simulating excitatory synaptic currents

Nonlinear, active filters generate the time and voltage dependent potassium and sodium conductances specified by Hodgkin and Huxley. The input to each of these filters is the simulated transmembrane potential. The output is a voltage or current representing the appropriate Hodgkin-Huxley conductance. Since the current through a conductor is proportional to the product of the conductance itself and the voltage across it, electronic multipliers are required in order to convert the filter outputs to equivalent conductances. The remaining two elements (G_L and C_M) of the Hodgkin-Huxley model are fixed and linear. These are simulated by simple electrical components. The time course of synaptic conductance is simulated by a simple resistor-capacitor network. The output of this network is transformed to an equivalent conductance by means of an electronic multiplier.

II. The Circuits

Five of the elements in the network of Fig. 1 depend on time or voltage or both. This section describes electronic-circuit realizations of those five elements. The five electronic circuits are combined with the two constant elements of Fig. 1 to provide the complete electronic model of a patch of neuronal membrane. The model was designed to simulate membrane potentials and currents in real time. The admittances were scaled to the actual values across a patch of membrane whose area is 0.25 cm^2. In order to make them compatible with the electronic circuits, however, the voltages and currents were increased over the values chosen by Hodgkin and Huxley (1952d, p. 520). The magnitude of the voltage and current scale factor depends on the application of the model. For full spike activity, the voltages and currents are taken to be eighty times the Hodgkin-Huxley values (see the table). For subthreshold activity, or activity with attenuated spikes, the voltages and currents are taken to be 120 times the Hodgkin-Huxley values, providing an expanded view of the potentials.

The circuits were designed for operation with the terminal representing the outside of the membrane grounded. In simulations of neuroelectric interactions between electrotonically connected regions of membrane, therefore, the resistances of intracellular pathways can be represented, but the resistances of extracellular pathways will be taken to be negligibly small. No provision has been made in the model for positive potentials at the terminal representing the inside of the membrane. When the voltage/current scale factor is taken to be 80 (i.e., voltages and currents in the model are 80 times their counterparts in the squid axon), the simulated sodium potential has been translated from +3.6 V (the value corresponding to Hodgkin's and Huxley's estimate of +45 mV) to 0 V. The potassium and leakage potentials have been translated an equal amount. When the voltage/current factor is taken to be 120, the simulated sodium potential is truncated at 0 V (representing 0 mV in the squid axon). Spikes that would carry the membrane potential beyond 0 mV also a re truncated (i.e., the spike amplitude is limited to 60 bis 65 mV). Other approximations and simplifications, including those related to voltage/current scale factor, are discussed in connection with the relevant circuits in the following sections.

A. Synaptic Shunt Conductance. The simulated synaptic shunt conductance is shown in Fig. 2. It is an approximation to a true time-dependent conductance. Over the range of potentials normally involved in synaptic responses, changes in the voltage across the equivalent shunt conductance are small in comparison to the voltage itself. In this range of potentials, therefore, the voltage across the shunt conductance reasonably can be considered constant, and the synaptic current can be taken to be directly proportional to the conductance alone. Under this approximation, the circuit that simulates the synaptic shunt conductance simply transforms a voltage pulse into a decaying exponential current. Then, rather than being applied to an electronic multiplier and converted into a true equivalent conductance, this current is applied directly across the simulated membrane.

During a positive pulse at the input of the synaptic circuit, the diode $D1$ conducts, and capacitor $C1$ is charged through resistor $R1$. The magnitude of $R1$ is variable and determines the amount of charge transferred to $C1$ during a pulse. In the absence of an input pulse, $C1$ discharges through variable resistor $R2$; the rate of discharge is determined by the magnitude of $R2$. The voltage on $C1$ is applied through an isolation amplifier ($Q1$ and $Q2$) and a resistor ($R5$) to the emitter of $Q3$. The output of $Q3$, a current proportional to the voltage on $C1$, is applied directly to the inside of the simulated membrane.

If the charge on $C1$ is considered to be analogous to chemical synaptic transmitter, then the voltage on $C1$ is analogous to the transmitter concentration. The

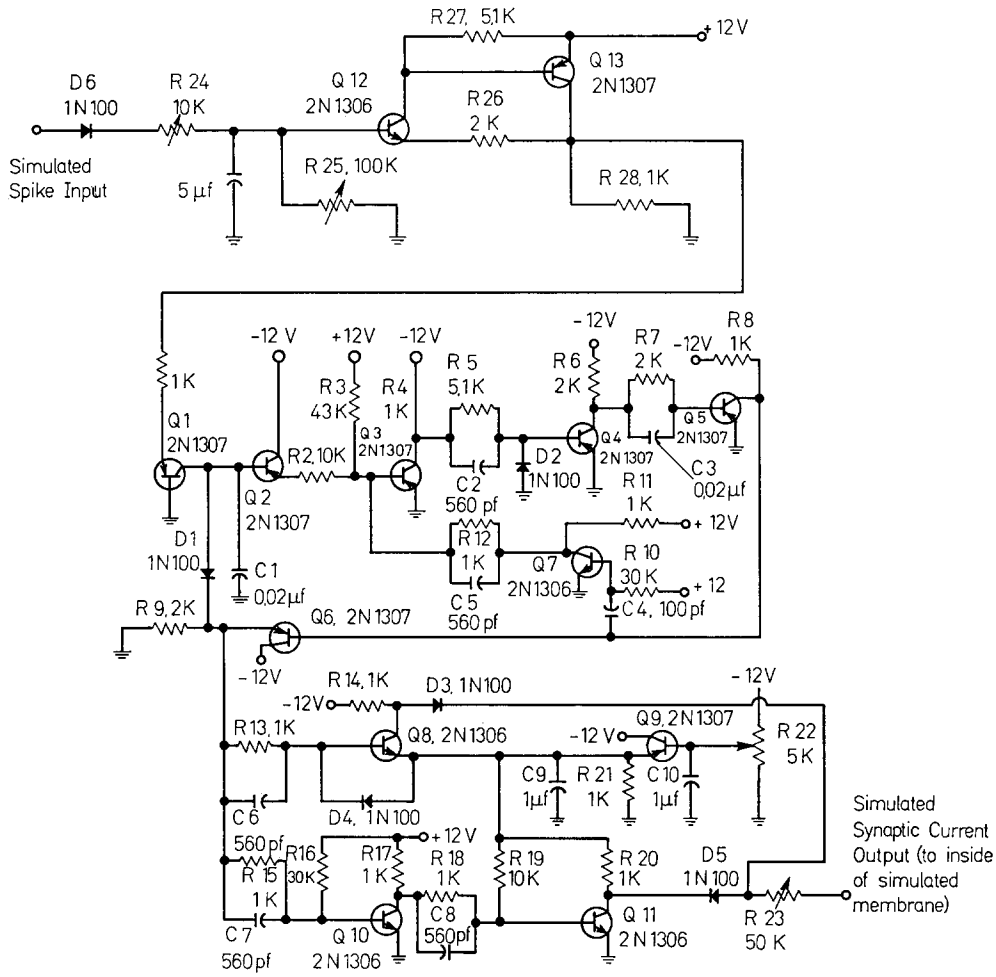

Fig. 3. An electronic circuit simulating synaptic chloride-ion conductance

charging of $C1$ through $R1$ is analogous to transmitter emission by the sending cell; and the discharge of $C1$ through $R2$ is analogous to first order inactivation of the transmitter. The simulated rates of emission and inactivation are determined by the magnitudes of $R1$ and $R2$ respectively.

B. Synaptic Chloride Conductance. Under ordinary circumstances the membrane potential is very close to V_{C1} (the reversal potential for chloride-ion flux); in fact the net driving force on chloride ions not only varies considerably in magnitude, but it often reverses its direction. Reasonable simulation of the time-varying synaptic component of chloride conductance requires a multiplier that can accommodate a reversal of the sign of one of its inputs. This is accomplished by the chloride conductance circuit shown in Fig. 3.

The circuit that simulates synaptic chloride conductance is divided functionally into three basic subcircuits — a pulse frequency modulator ($Q2$ to $Q7$), a pulse amplifier and inverter ($Q8$ to $Q11$), and a circuit that converts positive voltage pulses into decaying exponential current waveforms ($Q12$ to $Q13$). The last is identical to the circuit to the left of the emitter of $Q3$ in Fig. 2. Transistor $Q1$ serves as a summing point for decaying exponential current waveforms, and can accommodate several synaptic-time-course circuits. The collector current of $Q1$ is equal to the sum of those currents and is the input to the pulse frequency modulator. The pulse frequency modulator in this circuit is the exact electrical complement of the circuit described later for the simulated sodium conductance. The polarities of diodes and voltages in this pulse frequency modulator are the opposite of those in the pulse frequency modulator of the sodium circuit, and where a pnp transistor appears in one circuit, an equivalent npn transistor appears in the other. All capacitance and resistance values are identical in the two circuits and the operation is basically the same. The output of the chloride pulse frequency modulator is a series of negative twelve-volt pulses whose frequency is directly proportional to the sum of the currents applied to the emitter of $Q1$. The negative voltage pulses from the pulse frequency modulator are applied simultaneously to two channels in the pulse amplifier-inverter circuit. The simulated chloride potential (V_{C1}) is applied through a third channel. The amplifier inverter converts each pulse from the pulse-frequency modulator into two pulses, one going positive from -12 volts to the simulated chloride potential, the other going negative from ground potential to the simulated chloride potential. The simulated chloride potential itself is determined by the potentiometer $R22$. The voltage from this potentiometer is applied through an emitter follower ($Q9$) to the emitter of $Q8$ and the collector resistor of $Q11$. In the absence of a negative pulse at the emitter of $Q6$, -12 V appears at the collector of $Q11$. During a negative pulse, V_{C1} appears at both collectors. The resistor $R23$ is connected directly to the inside of the simulated membrane. Since the potential at this point is always between -12 V and the ground potential, diodes $D3$ and $D5$ are reverse-biased except during a pulse. If the simulated internal membrane potential is between V_{C1} and ground potential, $D5$ conducts during a pulse and $D3$ does not. If, on the other hand, the potential is between V_{C1} and -12 V, $D3$ conducts during a pulse and $D5$ does not. The current through $R23$ is thus equal to $(V_{C1}-V_M)/R23$ during a pulse and is equal to zero in the absence of a pulse; and the polarity of the current during a pulse is determined by the magnitude of V_M (the membrane potential) relative to the magnitude of V_{C1}. If the duration of each pulse is one microsecond, the maximum pulse frequency is 1 MHz. The average current through $R23$ over several pulses is

$$\frac{f}{10^6\,R23}\,(V_{C1}-V_M);$$

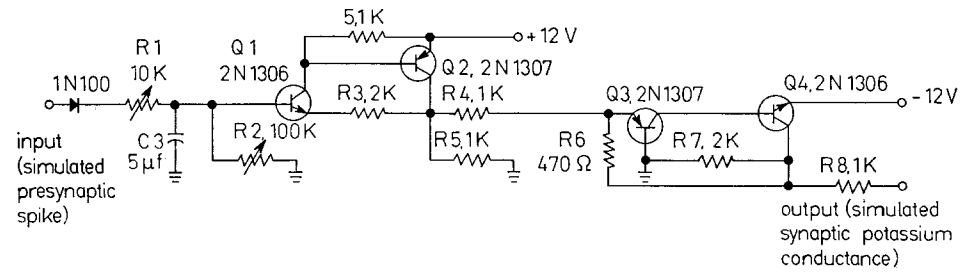

Fig. 4. An electronic circuit simulating the time course of synaptic potassium conductance

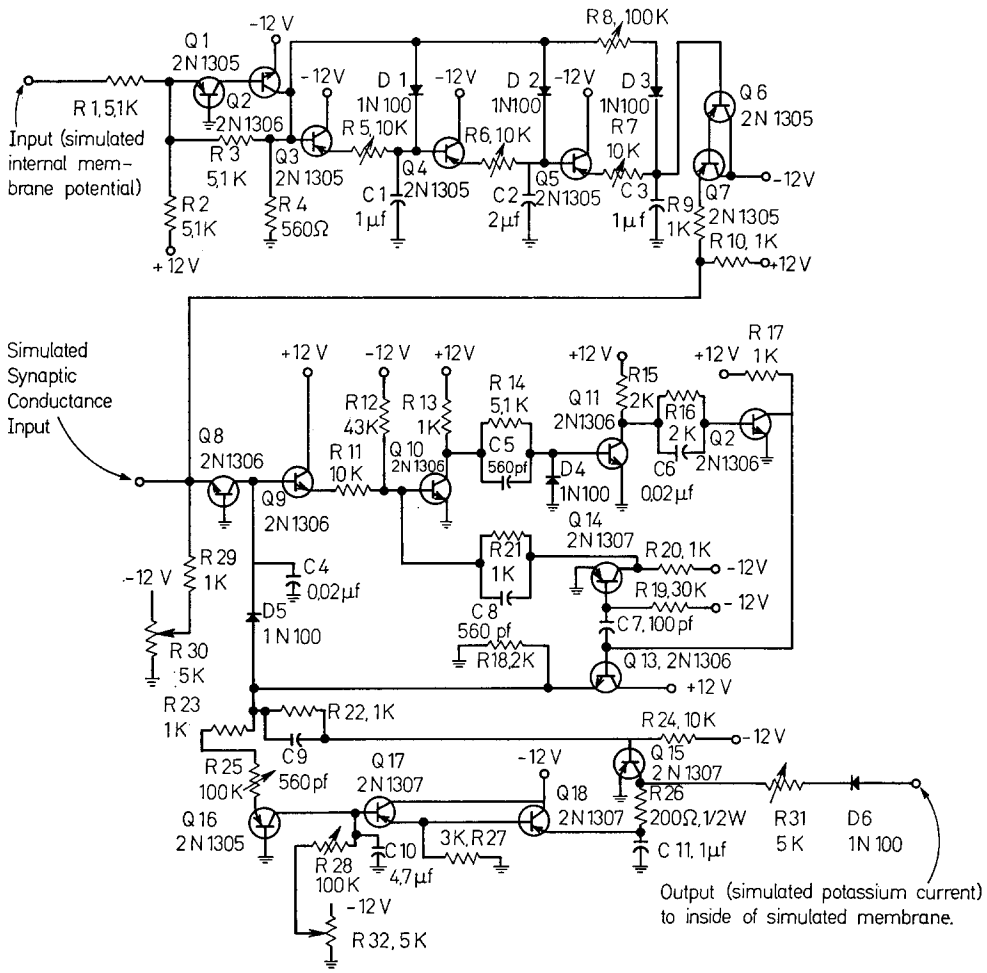

Fig. 5. An electronic circuit simulating the voltage-dependent potassium-ion conductance of the Hodgkin-Huxley description

where f is the pulse frequency. The equivalent synaptically induced chloride conductance becomes $f/10^6(R23)$ and is controlled by the variable resistor $R23$.

C. Synaptic Potassium Conductance. The circuit of Fig. 4 converts a positive voltage pulse into a negative, decaying exponential current. The portion of the circuit to the left of $R6$ in the figure is identical to the synaptic-time-course circuit in Fig. 2. This circuit converts positive voltage pulses into positive, decaying exponential current waveforms. The circuit to the right of $R6$ in Fig. 4 simply inverts these waveforms, making their polarity compatible with the input requirements of the pulse-frequency-modulator in the potassium circuit (Fig. 5). The decaying exponentials from the circuit of Fig. 4 are added to the simulated Hodgkin-Huxley component of potassium conductance, and the sum is effectively multiplied by $(V_K - V_M)$ through the pulse-frequency modulator of Fig. 5.

D. Membrane Capacitance and Leakage Conductance. The membrane capacitance and the Hodgkin-Huxley component of leakage conductance both are simulated by linear electrical components. The former is represented by a switchable capacitor (0.1 to 10 µF) connected from the inside of the simulated membrane to ground. The latter is represented by a variable resistor (50 kΩ) connected from the inside of the simulated membrane either to the chloride potential at the emitter of $Q9$ in the circuit of Fig. 3 or to a separate "leakage" potential.

E. Potassium Conductance. The circuit of Fig. 5 converts the time varying simulated membrane potential (V_M) into a current which in almost all respects is equivalent to the potassium current specified in the Hodgkin-Huxley description. The potassium circuit also provides for the addition of a simulated synaptic component of potassium current, as specified by

ECCLES and others. In the Hodgkin-Huxley formulation, the potassium current is the product of two variables and one constant:

$$I_K = \bar{g}_k(n^4)(V_K - V_M).$$

Where n^4 is a function of membrane potential and time; $\bar{g}_K$ is a constant; and V_K is the potential at which the potassium ion flux reverses, it is either constant or very slowly varying. The membrane potential (V_M) is normally close to V_K, and the difference between the two potentials ($V_K - V_M$) may vary considerably, even in the absence of spikes. Realistic simulation of the potassium current thus requires formation of the product of the two variables, (n^4) and ($V_K - V_M$). The potassium circuit is divided into three subcircuits. One of these generates a current representing n^4; another effectively forms the product of n^4 and ($V_K - V_M$): and the third provides optional dependence of V_K on the time integral of simulated potassium current.

In the n^4-generating circuit, V_M is applied through resistor $R1$ to the emitter of $Q1$. The combination of $Q1$ and $Q2$ is a linear, inverting amplifier whose output is $-(V_M + 12\,V)$. Since V_M is negative, the amplifier output varies between $-12\,V$ (for $V_M = 0$) and 0 (for $V_M = 12\,V$). The principal characteristic of the variable n^4 in the Hodgkin-Huxley model is its response to stepwise changes in V_M. For positive steps in V_M (step depolarizations of the membrane), n^4 rises in a sigmoid manner to a new, steady-state magnitude. In response to negative steps in V_M, n^4 falls in a nearly exponential manner. This combination of inflected rise and noninflected fall is simulated by the subcircuit beginning with $Q3$ and ending with $Q7$. Under static conditions, the voltage at the collector of $Q2$ i.e., $-(V_M + 12\,V)$ appears at the base and emitter terminals of each of the transistors $Q3$, $Q4$, $Q5$ and $Q6$. A positive step in V_M produces a negative step at the base of $Q3$, reverse-biasing the diodes $D1$, $D2$ and $D3$. The step is thus transmitted to the base of $Q6$ through the ladder network made up of $R5$-$C1$, $R6$-$C2$ and $R7$-$C3$. Measured at the base of $Q6$, the response to the step is sigmoid, with a degree of inflection determined by the values of the variable resistors $R5$, $R6$ and $R7$.

In response to a negative step in V_M, a positive step appears at the collector of $Q2$. The diodes $D1$, $D2$ and $D3$ become forward-biased, and the voltage at the collector of $Q2$ appears immediately at the base terminals of $Q4$ and $Q5$. The voltage at the base of $Q6$ rises exponentially toward the new value of $-(V_M + 12\,V)$ with a time constant determined by the value of variable resistor $R8$. Transistors $Q6$ and $Q7$ act together as an emitter follower to prevent loading effects on the n^4 generating circuit by the low input resistance of the following circuit (the pulse frequency modulator).

The final output representing n^4 is the sum of the currents through $R9$, $R10$, and $R29$. Under static conditions, the current through $R9$ is $(V_M + 12\,V)/1\,k\Omega$; the current through $R29$ is $V_0(G_K)/1\,k\Omega$, and the current through $R10$ is $12\,V/1\,k\Omega$. The sum of these currents represents the steady-state value of n^4 and is equal to $-(V_M - V_0(G_K))/1\,k\Omega$. This linear approximation to n^4 is compared in Fig. 6 with the Hodgkin-Huxley data. The magnitude of $V_0(G_K)$ is controlled by variable resistor $R30$. The collector current of $Q8$ is equal to the sum of the currents representing n^4 (i.e., the currents through $R9$, $R10$ and $R29$) as well as the current input from the synaptic circuit of Fig. 4. The pulse-frequency modulator ($Q9$ through $Q14$) is identical to that described for the sodium circuit. The frequency of positive 12 V pulses at the emitter of $Q13$ is directly proportional to the collector current of $Q8$.

The simulated potassium potential is the voltage at the collector of $Q16$. Under quiescent conditions, this voltage normally will be identical to that appearing at the wiper arm of potentiometer $R32$. If variable resistor $R25$ is set to its maximum value (approximately 100 kΩ) and variable resistor $R28$ is set to its minimum value (approximately zero), the simulated potassium potential will be constant and equal to the voltage at $R32$. If $R25$ and $R28$ are set to other values, the simulated potassium potential will be dependent on the time integral of the potassium current, just as it would in the case of a limited extracellular space (see FRANKENHAUSER and HODGKIN, 1956). This dependence in nerve cells is logarithmic; in the circuit it is approximated by a linear dependence.

Each positive voltage pulse at the emitter of $Q13$ produces a current pulse through diode $D6$. Each of these current pulses represents an increment of potassium current in this system. In addition to producing an increment of simulated potassium current at $D6$, each voltage pulse at the emitter of $Q13$ produces an incremental change in the simulated potassium potential at the collector of $Q16$. This change represents the effects of potassium-ion efflux from the nerve cell. The magnitude of the change is determined by the value of variable resistor $R25$. Restoration of the potassium potential is brought about by potassium-ion influx, simulated by the current through $R28$. The rate of restoration is determined by the setting of $R28$. Transistors $Q17$ and $Q18$ act together as an emitter-follower to provide the simulated potassium potential at capacitor $C11$ and resistor $R26$, without loading the collector circuit of $Q16$.

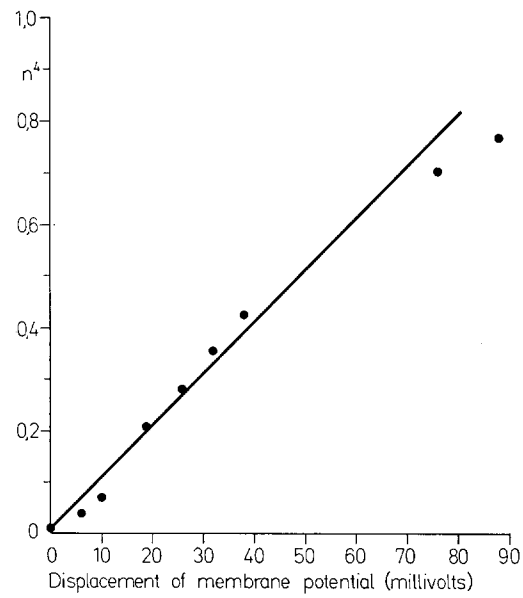

Fig. 6. The voltage dependence of the potassium conductance variable, n^4. The solid line is the linear approximation used in the model. The dots are taken from HODGKIN and HUXLEY (1952d). Positive voltages represents depolarizations, zero represents the resting potential

In the absence of a positive pulse at the emitter of $Q13$, transistor $Q15$ is on and its collector is at ground potential. During the occurrence of a positive pulse at $Q13$, transistor $Q15$ is off and the simulated potassium potential appears at its collector. The voltage waveform at $R31$ is thus a series of negative pulses, each starting at the ground potential and each having an amplitude equal to V_K. These pulses are applied through resistor $R31$ to diode $D6$. In the absence of a negative voltage pulse at $R31$, $D6$ is off and no current flows through $R31$. During a pulse, on the other hand, $D6$ is forward biased and a pulse of simulated potassium current flows to the point representing the inside of the membrane. The current (I_K) through $D6$ is described by the following expressions:

$$I_K = 0 \qquad \text{in absence of a pulse at } Q15;$$

$$I_K = \frac{V_K - V_M}{R31} \qquad \text{during a pulse at } Q15.$$

The frequency of pulses at $Q15$ is directly proportional to the sum of the two simulated components of potassium conductance, the electrically excitable component which is proportional to n^4, and the synaptic component. In the case of one-microsecond pulses at $Q15$, the maximum pulse frequency is 10^6 Hz, and the average current through $D6$ over several pulse periods is given by

$$(I_K) = \frac{f}{10^6}\,\frac{V_K - V_M}{R31};$$

Where V_K is the potassium potential; $R31$ is the resistance of variable resistor $R31$; and f is the pulse frequency. The

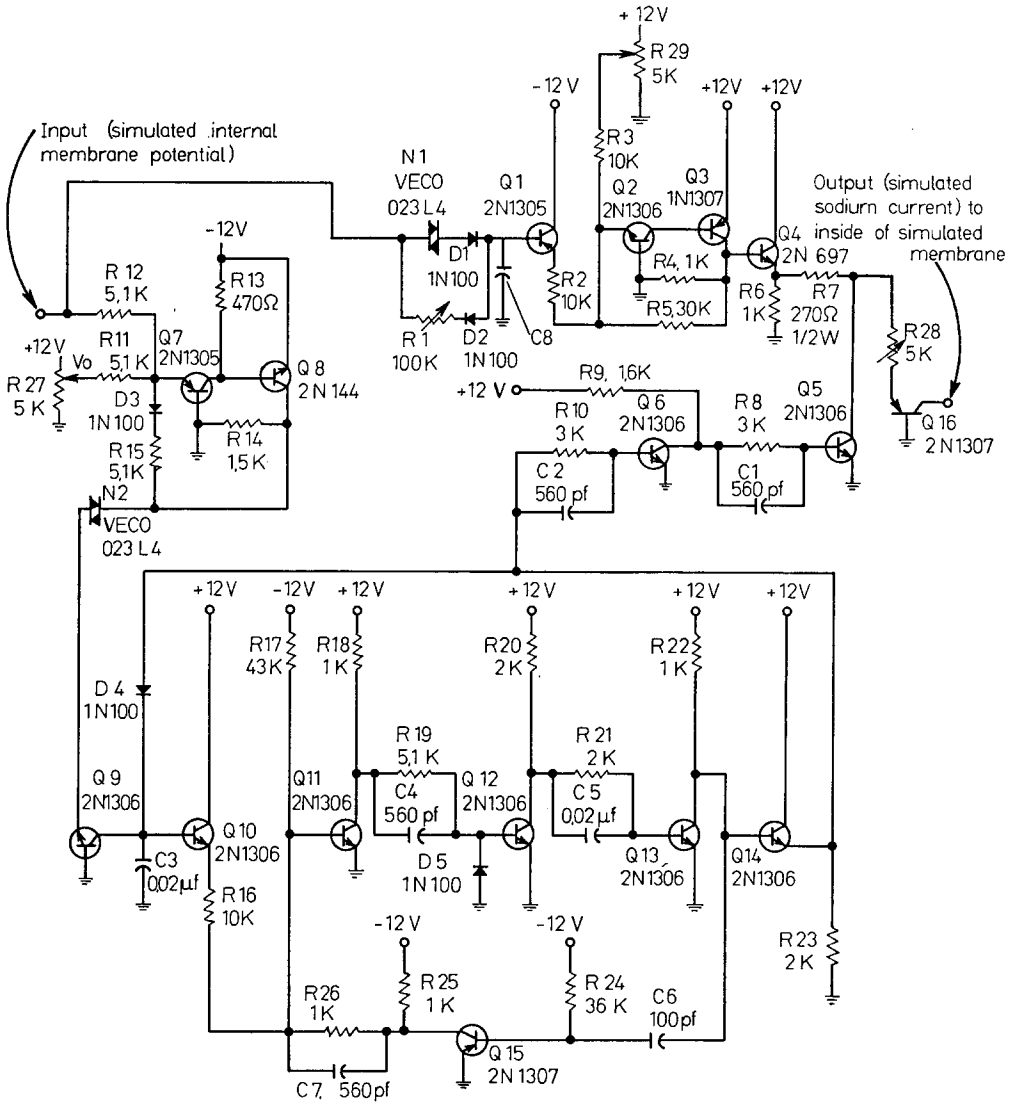

Fig. 7. An electronic circuit simulating the voltage-dependent sodium-ion current of the Hodgkin-Huxley description

equivalent potassium conductance in this system becomes equal to $f/10^6\ R31$. Resistor $R31$ thus provides simultaneous control over the magnitudes of both simulated potassium conductance components. Independent control of the synaptic component is achieved by variation of $R1$ in Fig. 4.

F. Sodium Conductance. The circuit of Fig. 7 converts the time-varying simulated membrane potential (V_M) into a current that in almost all respects is equivalent to the sodium current specified in the Hodgkin-Huxley description. In their formulation, the sodium current is the product of three variables and one constant:

$$I_{Na} = \bar{g}_{Na}(m^3)(h)(V_{Na} - V_M)$$

where m^3 and h are functions of membrane potential and time; $\bar{g}_{Na}$ is a constant; and V_{Na} is the potential at which the net sodium ion flux reverses direction, it also is constant. Except during a spike, the factor $(V_{Na} - V_M)$ is large compared to changes in V_M and can be considered constant. During a spike, V_M quickly approaches V_{Na}, passing rapidly through the range of potentials intermediate between the threshold and V_{Na}. The variations in $(V_{Na} - V_M)$ in this range probably are not important in determining the electrical properties of the Hodgkin-Huxley model; on the other hand, the limiting effect imposed upon the sodium current as V_M approaches V_{Na} is important. In the sodium circuit, $(V_{Na} - V_M)$ is treated as a constant over the entire range of membrane potentials; but the limiting effect of the factor is included, so that the simulated sodium current approaches zero as V_M approaches V_{Na}. The principle functions of the sodium circuit, therefore, are to generate the time and voltage dependent functions m^3 and h and to generate a current proportional to their product.

The membrane potential is applied to the inputs of two subcircuits. One subcircuit ($Q1$ to $Q4$) generates a voltage representing h, the other ($Q7$ to $Q9$) generates a current representing m^3. The remaining circuit ($Q5$, $Q6$, $Q10$ to $Q14$) acts as a multiplier, generating a pulsed output voltage whose average over time represents hm^3. In the h-generating circuit, V_M is applied through $R1$, $D1$, $D2$, and $N1$ (a varistor) to capacitor $C8$. The voltage on this capacitor tends to follow V_M, but lags it in time. The varistor $N1$ provides an approximation to the voltage-dependent rate of decline of h in response to positive changes in V_M. The variable resistor $R1$ determines the rate of increase of h in response to negative changes in V_M. Both rate constants can be scaled simultaneously by means of switched capacitors ($C8$). Fig. 8 shows for typical settings of $R1$ and $C8$ a family of voltage outputs appearing at the emitter of $Q4$ in response to sudden step changes in the simulated membrane potential. The portion of the circuit from $Q1$ through $Q4$ is simply an amplifier that provides a piecewise linear approximation of the steady-state magnitude of h as a function of V_M, as shown in Fig. 9. Transistor $Q1$ is an emitter-

follower, supplying the voltage at $C8$ to $R2$ without significantly loading the capacitor. Transistors $Q2$ and $Q3$ together act as an inverting amplifier with a gain of 3. The effective input to this amplifier is the sum of the voltage at $C8$ and that on the wiper arm of potentiometer $R29$. When this sum is positive, the output of the amplifier (i.e., the collector of $Q3$) is at ground potential. When the input sum is between ground potential and -4 V, the magnitude of the amplifier output is three times the sum, with positive polarity. When the input sum is more negative than -4 V, the amplifier output is $+12$ V. The amplifier thus has the response curve shown by the solid line in Fig. 9. This curve can be shifted along the horizontal axis by adjustment of potentiometer $R29$. Transistor $Q4$ is an emitter follower supplying the amplifier output to the low resistance load ($R7$).

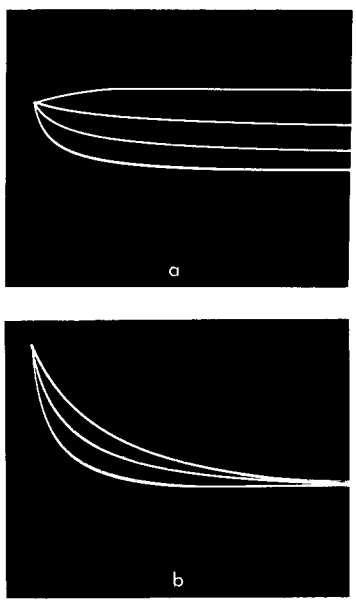

Fig. 8 a and b. The time courses of sodium inactivation simulated by the circuit of Fig. 7 for stepwise changes in membrane potential. From top to bottom the traces show the responses to a 10-mV hyperpolarizing step in a and the responses to depolarizing steps of 10, 20 and 30 mV respectively in a and b. b shows the three depolarization responses normalized in amplitude and expanded in time to show the voltage-dependent rates of fall

In the m^3-generating circuit, V_M is applied through $R12$ to the emitter of $Q7$. Transistors $Q7$ and $Q8$ together act as an inverting amplifier with unity gain. The output at the collector of $Q8$ is positive in polarity and equal in magnitude to the sum of the simulated membrane potential and the voltage on the wiper arm of potentiometer $R27$. The amplifier output is applied through the varistor $N2$ to the emitter of $Q9$. The varistor imposes a nonlinear relationship between $V_M + V_0$ and the collector current of $Q9$. This relationship is intended to simulate the nonlinear dependence of m^3 on the displacement of the membrane potential from equilibrium, see Fig. 10. The rise time of m^3 in the electronic model is taken to be zero, however (see Section III A); so the peak simulated sodium conductance is independent of changes in h and depends only on m^3. To compensate for this lack of dependence on h, I have assigned values to m^3 that are directly proportional to the peak sodium conductance (Hodgkin and Huxley, 1952a, p. 464, axon 17). The simulated dependence of m^3 on membrane potential can be improved for specific situations by variation of $R11$. When the voltage/current scale-factor equals 80, for example, 6.8 kΩ is a better value for $R11$. When the scale factor equals 120, a good match at very low voltages is provided by a 10 kΩ resistor (see Fig. 10). Variation of $R27$ shifts the curve to the right or left without altering its shape.

The subcircuit from transistor $Q10$ to transistor $Q15$ is a pulse-frequency modulator. It generates 1- to 2-microsecond, 12 V pulses whose frequency is directly proportional to the current into capacitor $C3$ from the collector of $Q9$. Immediately after the occurrence of a pulse at the emitter of $Q14$, capacitor $C3$ is positively charged and $+12$ V appears at the base of $Q10$. Transistor $Q10$ is an emitter-follower, supplying the voltage at $C3$ to $R16$ without significantly draining the charge on $C3$. The rate of discharge of $C3$ is thus almost entirely determined by the collector current of $Q9$; if this current is constant, the voltage on $C3$ falls linearly from $+12$ toward the ground potential. As long as the voltage on $C3$ is greater than approximately $+3$ V, transistor $Q11$ remains on, and its collector is at ground potential. While $Q11$ is on, the following conditions exist: The collector of $Q12$ is at $+6$ V; the collector of $Q13$ and the emitter of $Q14$ are both at ground

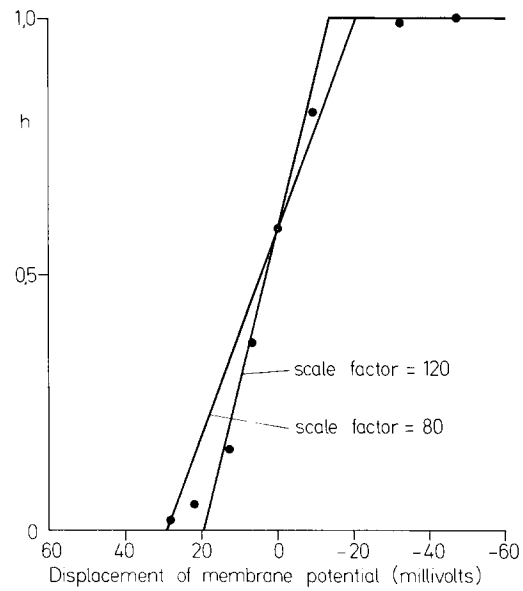

Fig. 9. The dependence on membrane potential of the Hodgkin-Huxley sodium inactivation variable, h. The dots are data taken from Hodgkin and Huxley (1952c); the solid lines show the piecewise linear approximations employed in the model

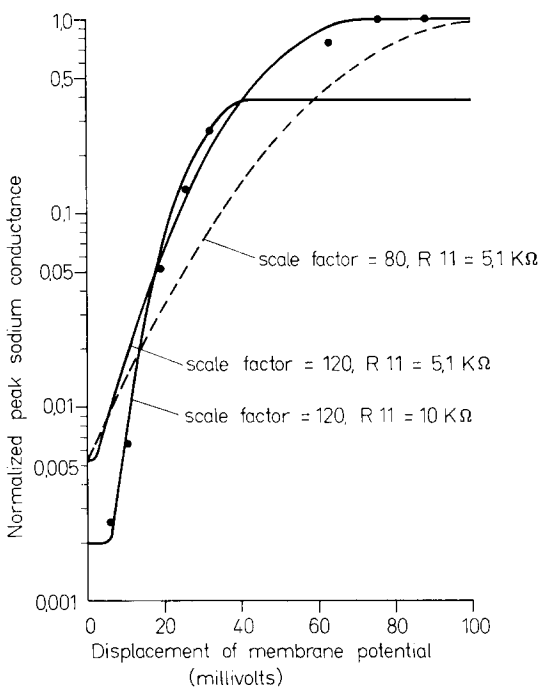

Fig. 10. The dependence on membrane potential of the Hodgkin-Huxley sodium activation variable, m^3. The dots are data taken from Hodgkin and Huxley [Fig. 9, p. 464 (1952a)]. The lines show various approximations employed in the model

potential; diode $D4$ is reverse-biased and therefore not conducting; and transistor $Q15$ is on, and its collector is at ground potential.

When the voltage on $C3$ has fallen below $+3$ V, $Q11$ turns off, and $+10$ V appears at its collector. Transistor $Q12$ is turned on, driving $Q13$ off, $+12$ V suddenly appears at the collector of $Q13$ and the base of $Q15$. As capacitor $C6$ is charged through $R24$, the voltage on the base of $Q15$ falls from its initial positive value toward -12 V. As long as the base voltage of $Q15$ is positive, its collector is at -12 V. During this time, $Q11$ is held in the nonconducting state and $+12$ V appears at the collector of $Q13$ and the emitter of $Q14$. The positive voltage at the emitter of $Q14$ causes $D4$ to conduct, recharging $C3$ to $+12$ V. The duration of the positive emitter voltage at $Q14$ is determined by the combination of $R24$ and $C6$. When the voltage at the base of $Q15$ reaches the ground potential, $Q15$ turns on. This causes $Q11$ to turn on, driving $Q12$ off and $Q13$ on. The collector voltage of $Q13$ and the emitter voltage of $Q14$ both return to the ground potential, terminating the output voltage pulse. The next pulse occurs after a time determined by the collector current of $Q9$.

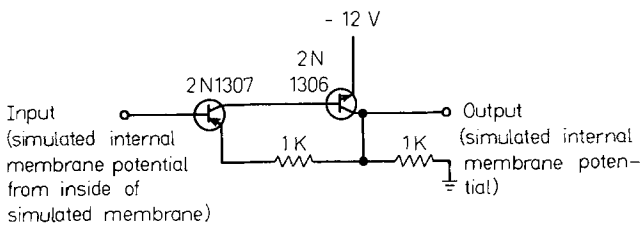

Fig. 11. An isolation amplifier to provide the simulated membrane potential to various circuits without altering the properties of the simulated membrane itself

The voltage waveform at $C3$ is a saw-tooth, varying between $+12$ V and $+3$. Its frequency is directly proportional to the collector current of $Q9$.

Transistors $Q5$ and $Q6$ act as pulse amplifiers. The collector voltage of $Q6$ normally is $+12$ V, while the collector of $Q5$ is at ground potential. When a positive pulse appears at the emitter of $Q14$, the collector of $Q6$ is switched to ground potential and the voltage output of the h-generating circuit suddenly appears at the collector of $Q5$. The waveform at $Q5$ is thus a positive, one- to two-microsecond pulse whose amplitude is proportional to h and whose frequency is proportional to m^3. The average voltage at the collector of $Q5$ is directly proportional to m^3h. This voltage is converted by $Q16$ to a current whose average value is proportional to m^3h. The magnitude of the current is controlled by variable resistor $R28$.

G. Isolation of the Membrane Potential. The simulated membrane potential serves as the input variable for the sodium- and potassium-conductance circuits. If the input terminals of these circuits were connected directly to the node representing the inside of the membrane, the circuits would load the simulated membrane and significantly alter its properties. This loading effect is eliminated when the simulated membrane potential is applied to the circuit inputs through the isolation amplifier of Fig. 11.

III. Controllable Parameters in the Circuit

When the circuits of Figs. 2—5, 7 and 11 are connected in the manner indicated in the figures, the resulting model represents the configuration of Fig. 1. As it is described in Section II, the model has 24 controls, 22 of which are variable resistors or potentiometers and two of which are switched capacitors. Seven of the controls are related to the synaptic portion of the model (i.e., the portion on the left side of the dashed line in Fig. 1); the remaining seventeen controls are related to the electrically excitable portion of the circuit (on the right side of the dashed line). Although this array of controllable parameters is formidable, it is not impossible to manage, even when several of the models are interconnected to represent distributed neuroelectric processes within a single nerve cell. One strategy that makes the system tractable, for example, is that under which the parameters of each model are adjusted to a basic configuration matching as closely as possible the specifications of Hodgkin and Huxley for the squid giant axon. Small parameter changes can be treated as perturbations of that basic configuration. When several models are interconnected to represent small neural networks, the synaptic parameters become important. Each simulated synapse effectively has only two parameters, however, and the response of the whole network usually is not critically dependent on these. A good strategy for dealing with networks seems to be first to establish and fix the parameters of the electrically excitable portion of each model, then to experiment with the synaptic parameters alone.

A. Specifications of the Hodgkin-Huxley Model. Most of the membrane conductance data published by Hodgkin and Huxley were inferred from experiments in which the transmembrane potential was suddenly changed and held at a new value, and the time course of the resulting transmembrane current was observed. For that reason the parameters are discussed here in terms of conductance changes in response to a suddenly applied voltage step. The parameters apply to the giant axon of the squid at 6° C. As mentioned in Section I A, Hodgkin and Huxley found that in response to a stepwise change in the membrane potential, the time course of the sodium conductance was described reasonably accurately by the following equation:

$$G_{\mathrm{Na}} = \bar{g}_{\mathrm{Na}} m^3 h \tag{1}$$

where $\bar{g}_{\mathrm{Na}}$ is a constant amplitude factor; $m(t)$ is a rising negative exponential; and $h(t)$ is a decaying exponential. They found that the potassium conductance was described accurately by the following equation:

$$G_{\mathrm{K}} = \bar{g}_{\mathrm{K}} n^4 \tag{2}$$

where $\bar{g}_{\mathrm{K}}$ is a constant, amplitude factor; and $n(t)$ is a rising negative exponential. The membrane capacitance and leakage conductance were found to be constant (independent of time and voltage). The time dependent variables are described by the following equations:

$$m(t) = m_\infty - (m_\infty - m_0)\exp(-t/\tau_m), \tag{3}$$

$$h(t) = h_\infty - (h_\infty - h_0)\exp(-t/\tau_h), \tag{4}$$

$$n(t) = n_\infty - (n_\infty - n_0)\exp(-t/\tau_n) \tag{5}$$

where m_0, h_0 and n_0 depend only on the initial value of membrane potential (before the stepwise change); m_∞, h_∞, n_∞, τ_m, τ_h, and τ_n depend only on the final value of membrane potential (after the stepwise change).

The forms of the simulated voltage dependencies of n_∞, m_∞, and h_∞ are fixed in the electronic model of Section II (see Figs. 6, 9 and 10); but the values of m_0, h_0 and n_0 at the resting potential are adjustable. τ_m generally is less than 0.5 ms, and changes in m are

much more rapid than changes in any other variable in the Hodgkin-Huxley formulation (including membrane potential); so τ_m is taken to be zero in the simulation. HODGKIN and HUXLEY measured the voltage dependence of τ_h and τ_n for stepwise reductions in membrane potential (depolarizations); but their data for stepwise increases (polarizations) is incomplete. In the electronic model each of these parameters (τ_h and τ_n) is divided into two independent parameters, a time constant for depolarization and a time constant for polarization. In the case of τ_h, we have designated the time constant for depolarization τ_i (the time constant of sodium-conductance inactivation); the corresponding time constant for polarization is designated τ_r (time constant of recovery from inactivation). Fig. 12 shows τ_i as a function of membrane potential for a typical squid axon (HODGKIN and HUXLEY, 1952b). HODGKIN and HUXLEY (1952c) measured τ_r for only one case, repolarization from 44 mV below the resting potential (i.e., a step change from approximately -16 mV to approximately -60 mV); τ_r in this case was 12 ms. The voltage dependence of τ_n for depolarization is shown in Fig. 13. The corresponding time constant for polarization is designated τ_n^*. HODGKIN and HUXLEY observed that in cases of repolarizations from various potentials to the resting potential, τ_n^* was essentially constant at approximately 5 ms. For polarizations to depolarized states, τ_n^* was slightly shorter.

In addition to the aforementioned parameters, which are from Eqs. (3), (4) and (5), two parameters, $\bar{g}_{Na}$ and $\bar{g}_K$, from Eqs. (1) and (2) are adjustable in the electronic model. Finally, the leakage conductance (G_L), the membrane capacitance (C_m), the potentia at which potassium-ion current reverses (V_K), and the potential at which the leakage current reverses (V_L) all are adjustable. The table is a list of these parameters, their values according to the Hodgkin-Huxley data, and the settings of the controls in the model that provide those values.

B. Other Parameters. In addition to controls related to the Hodgkin-Huxley parameters, the electronic model has controls related to synaptic parameters and controls related to variations of the potassium potential (V_K). In each simulated synaptic conductance, the increment of conductance change per presynaptic spike is controllable ($R1$ in Fig. 2, $R24$ in Fig. 3, $R1$ in Fig. 4); and the rate of synaptic conductance decline also is controllable ($R2$ in Fig. 2, $R25$ in Fig. 3, $R2$ in Fig. 4). The magnitude of the simulated synaptic leakage conductance has a second control in the model ($R22$, Fig. 3). This resistor should be set at 50 kΩ when the synaptic leakage conductance is not being used. The rate of simulated decline of V_K during efflux of potassium ions is controlled by $R25$. If the decline of V_K is to be neglected, $R25$ should be set at 100 kΩ, $R28$ should be set at 0.

C. Oscillatory Potentials: An Example of Systematic Parameter Variations. The parameters of the electronic model were adjusted to the values specified in the table, so that it represented a patch of squid-axon membrane for large excursions of membrane potential (i.e., $R5$, $R6$ and $R7$ of Fig. 5 were set at 200, 400 and 600 Ω respectively). A steady depolarizing current was applied across the simulated membrane. As this current was increased, oscillations appeared at the node

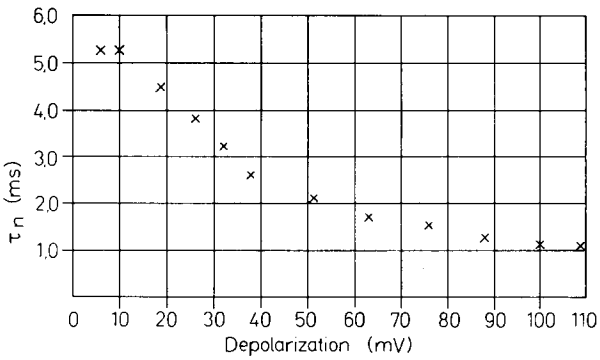

Fig. 12. Voltage dependence of the time constant of sodium inactivation [taken from HODGKIN and HUXLEY (1952d)]

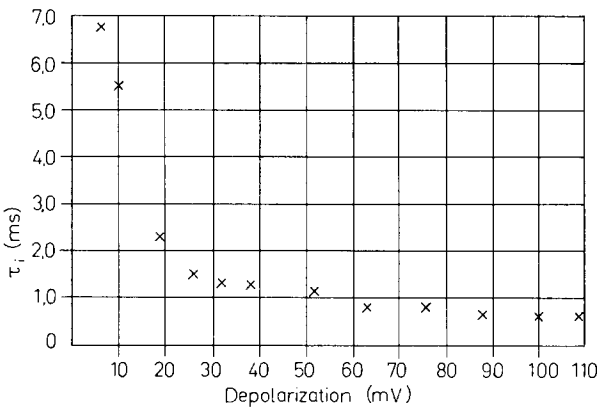

Fig. 13. Voltage dependence of the time constant of potassium-conductance increase [taken from HODGKIN and HUXLEY (1952d)]

Table. *Specifications of the Hodgkin-Huxley model for a 0.25-cm² patch of squid-axon membrane*

Hodgkin-Huxley-Parameter	Value specified by HODGKIN and HUXLEY	Control in electronic model	Setting of control that provides specified value
m_0	0.042	$R27$ (Fig. 7)	7 to 8 V (on wiper arm)
h_0	0.6	$R29$ (Fig. 7)	3 V (on wiper arm)
$\tau_i(\tau_h)$	voltage dependent 0.67 to 6.7 ms	voltage dependence shifted by $C8$ (Fig. 7)	1 μF
$\tau_r(\tau_h)$	12 ms	$R1$ (Fig. 7)	12 kΩ (when $C8 = 1$ μF)
τ_n	voltage dependent 1.0 to 5.25 ms	$R5$, $R6$, $R7$ (Fig. 5)	For spikes: 200, 400, 600 Ω. For subthreshold potential: 1, 2, 3 kΩ
$\tau_n^*(\tau_n)$	2.5 to 5.0 ms	$R8$ (Fig. 5)	5 kΩ
$\bar{g}_{Na}$	30 mmho	$R28$ (Fig. 7)	0
$\bar{g}_K$	9 mmho	$R31$ (Fig. 5)	0
G_L	0.07 mmho	separate resistor (Section II D)	14 kΩ
C_M	0.25 μF	separate capacitor (Section II D)	0.25 μF
V_K	-127 mV (referred to V_{Na})	$R32$ (Fig. 5)	-10 V
V_L	-105 mV (referred to V_{Na})	$R22$ (Fig. 3)	-8 V

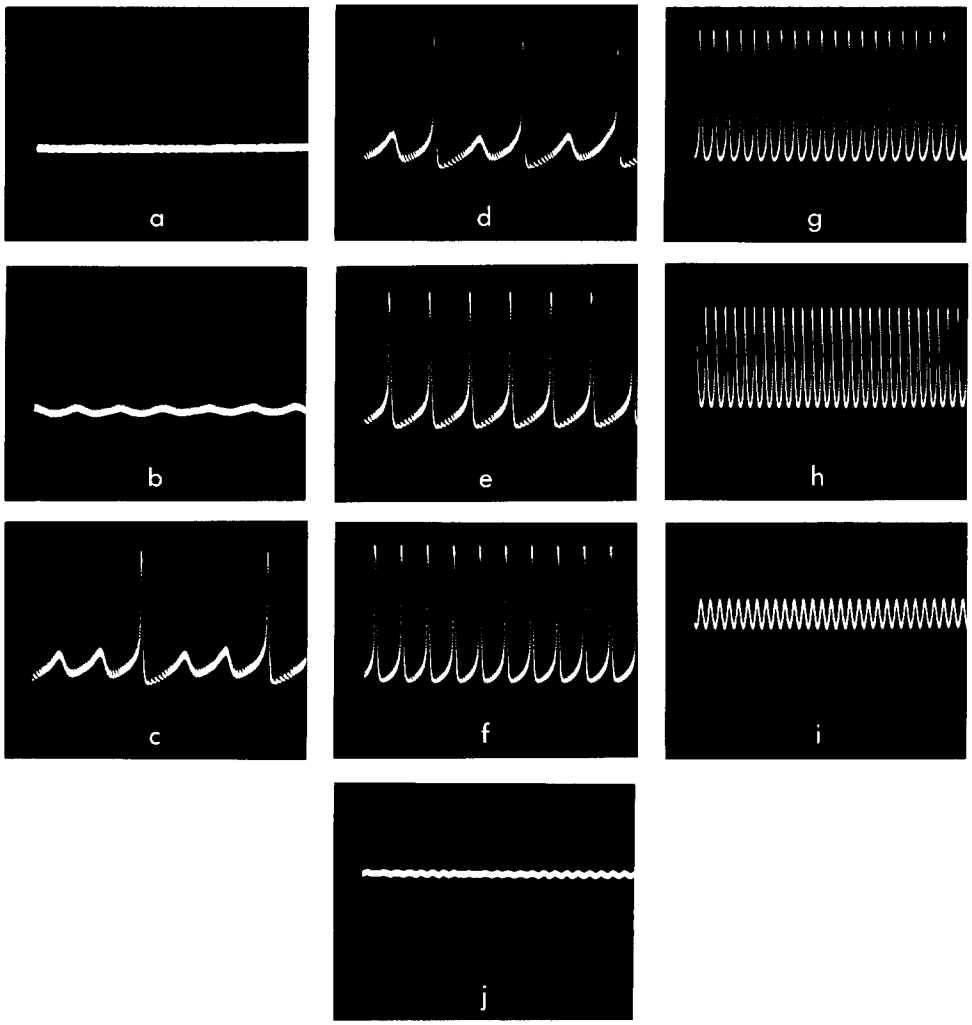

Fig. 14. Periodic variations in simulated membrane potential elicited by application of positive *dc* current to the node representing the inside of the membrane. The current was increased progressively from *a* to *j*. See text

representing the inside of the membrane. With further increase of the current, the oscillations became spikes whose frequency increased monotonically with increasing current. When the spike frequency was approximately 100 Hz, it no longer increased. Instead, the spike amplitude diminished and the response reverted to small oscillations. With further increase in the current, the oscillations disappeared. At this point the simulated membrane potential was the equivalent of approximately 30 mV below the resting potential. This sequence of events is shown in the photographs of Fig. 14. Periodic activity of the type shown in Fig. 14 can be induced in the model by any mechanism that tends to depolarize the membrane and prevent maintenance of the resting potential. The system described by the Hodgkin-Huxley data is inherently unstable and includes several possible oscillatory modes. Many of these have been described in considerable detail in an earlier publication (Lewis, 1966). When the parameters of the electronic model were adjusted to match the Hodgkin-Huxley data for large excursions, the minimum frequency of the subthreshold oscillations was approximately 50 Hz. Since a spike did not necessarily occur on every cycle of the oscillation, the minimum spike frequency was considerably less than 50 Hz. The minimum spike frequency with stable operation, however, was approximately 16 Hz.

For depolarizations less than 20 mV in the squid axon, the time "constant", τ_n, for the increase of potassium conductance is nearly constant at 5 ms (see Fig. 13). The corresponding time constant in the electronic model is equal to 5 ms when $R5$, $R6$ and $R7$ of Fig. 5 are set at 1, 2 and 3 kΩ, respectively. With τ_n in the model increased from 1 to 5 ms, the spike duration is approximately doubled and the slope of the repolarizing phase is considerably reduced. The minimum frequency for subthreshold oscillations is reduced from 50 Hz to approximately 25 Hz, but these oscillations are much less stable and are more likely to develop into full spikes. This instability is due to the inability of the slowed potassium conductance to overtake and arrest the regenerative action of the sodium conductance before the occurrence of a spike. Since with τ_n equal to 5 ms the parameters of the model are very close to those specified by Hodgkin and Huxley for small excursions of potential across the squid-axon membrane, subthreshold oscillations in that system also should be unstable.

In the squid axon, the rate of decline of the potassium conductance was nearly constant at approximately 0.20 ms^{-1} for excursions of membrane potential less than 30 mV and for rapid repolarization to potentials within 30 mV of the resting potential (Hodgkin and Huxley, 1952b, p. 492). In the model

this rate constant is treated in terms of its reciprocal, the time constant τ_n^* in the table. The value of τ_n^* according to the Hodgkin-Huxley data is 5 ms. With τ_n (the time constant for the increase of potassium conductance) set equal to 5 ms, τ_n^* (the time constant for decline of the potassium conductance) was varied from 5 to 80 ms. The effects of this variation on spontaneous spikes are shown in Fig. 15. The spike frequency decreased with increasing magnitudes of τ_n^*, from 50 spikes per second when $\tau_n^* = 5$ ms to 7 spikes per second when $\tau_n = 80$ ms. The spike frequency was not linearly related to τ_n^* since a 16-fold increase in τ_n^* brought a 7-fold reduction in frequency.

With τ_n and τ_n^* both equal to 5 ms, the simulated membrane capacitance in the model was increased to 1.0 μF (the equivalent of 4 μF/cm² in the squid axon). A steady depolarizing current applied to the model produced the oscillatory potentials shown in Fig. 16a. These potentials could be described as attenuated spikes, since they exhibited an all-or-nothing characteristic. In other words, this periodic waveform was stable in form and amplitude, and changed only in frequency as the magnitude of the depolarizing current was varied. Once again τ_n^* was varied from 5 to 80 ms, and the effects are shown in the photographs of Fig. 16. The amplitude of the waveform was constant and its all-or nothing nature persisted until τ_n^* was increased beyond 20 ms. When τ_n^* was 40 ms, the amplitude of the oscillations was reduced to the equivalent of approximately 20 mV in the squid axon, and their frequency was approximately 8 Hz.

With τ_n and τ_n^* both equal to 5 ms, the simulated membrane capacitance was increased again, this time to 2 μF (8 μF/cm² in the squid). The amplitude of the oscillations was completely graded, depending on the magnitude of the depolarizing current. The frequency of these oscillations increased monotonically with increasing current. Their amplitude, on the other hand, was a nonmonotonic function of depolarizing current, increasing as the current was increased from low magnitudes, passing through a maximum equivalent to approximately 30 mV, then decreasing as the current was increased further. The amplitude of these oscillations is plotted against their frequency in Fig. 17. The depolarizing current was fixed at a magnitude that induced an 8 Hz oscillation with an amplitude equivalent to approximately 20 mV, as shown in Fig. 18a. Then τ_n^* was increased from 5 to 80 ms, and the results also are shown in Fig. 18. As τ_n^* was increased, the amplitude of the oscillation increased, and the frequency decreased.

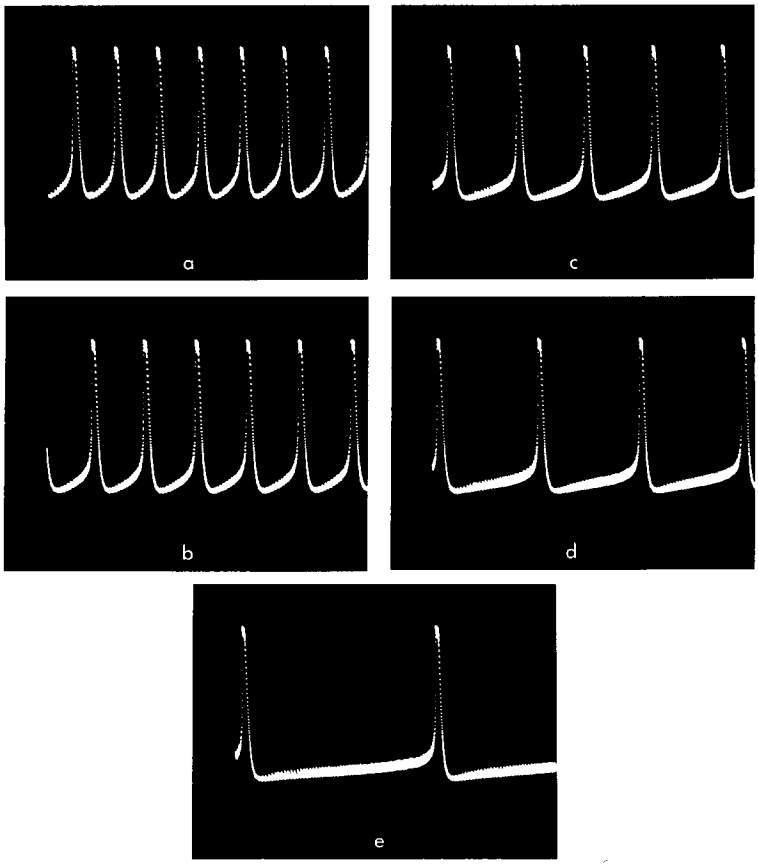

Fig. 15. Periodic spikes for various magnitudes of τ_n^*. The magnitudes of τ_n^* were as follows: a 5 ms; b 10 ms; c 20 ms; d 40 ms; e 80 ms

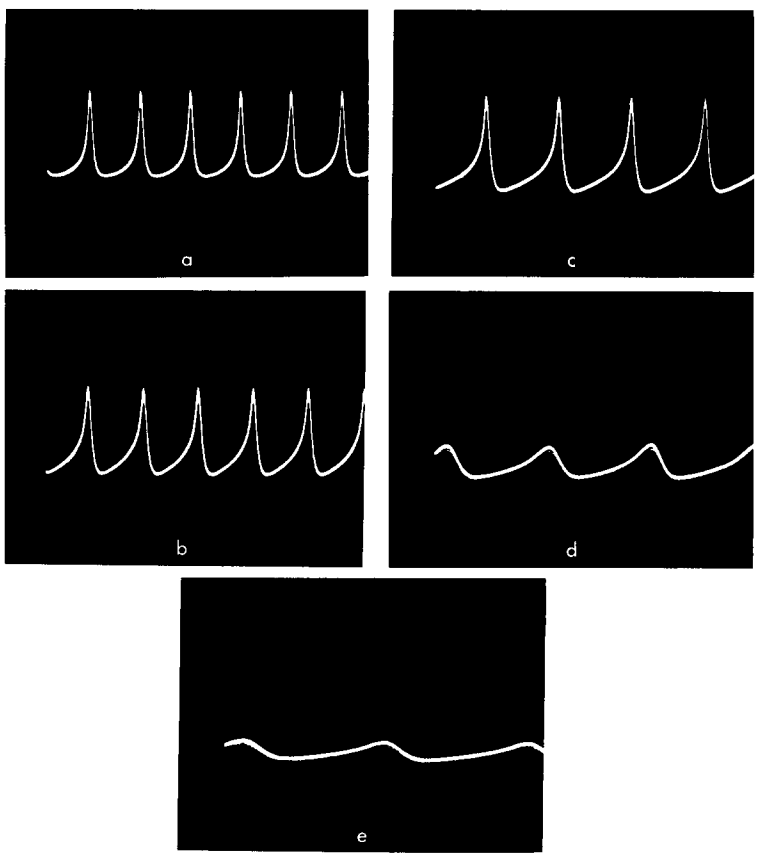

Fig. 16. Periodic oscillations of simulated membrane potential for various magnitudes of τ_n^*, with the simulated membrane capacitance increased by a factor of four over the magnitude specified by Hodgkin and Huxley. The magnitudes of τ_n^* were as follows: a 5 ms; b 10 ms; c 20 ms; d 40 ms; e 80 ms

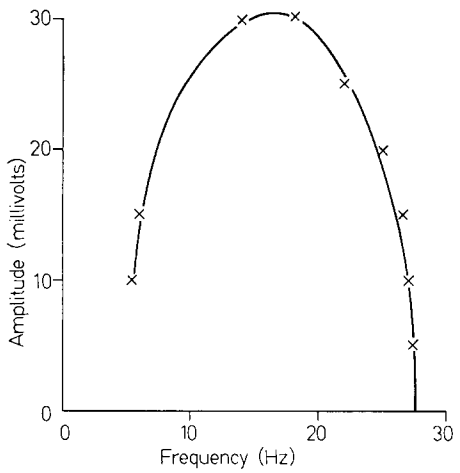

Fig. 17. Amplitude as a function of frequency for subthreshold oscillations induced by *dc* depolarizing currents in the model. The simulated membrane capacitance was eight times the magnitude specified by Hodgkin and Huxley

When τ_n^* was equal to 80 ms, the amplitude was equivalent to approximately 30 mV and the frequency was approximately 4 Hz.

In their mathematical formulation of the squidaxon data, Hodgkin and Huxley assumed that the rate of rise and the rate of fall of the potassium conductance were related. The solution of their equation for the potassium conductance variable, n, in response to a sudden change in membrane potential was

$$n = n_\infty - (n_\infty - n_0)\, e^{-t/\tau_n}$$

where n_0 is the initial value of n, and n_∞ is its final value. They related the potassium conductance to n by

$$G_K = \bar{g}_K\, n^4; \qquad (6)$$

where $\bar{g}_K$ is a constant. In the case of depolarizations, n_∞ is greater than n_0, so the potassium conductance has the same form as $(1 - e^{-t/\tau_n})^4$, which is an inflected rise to a constant value, 1.0. In the case of repolarization, n_0 is greater than n_∞, so the potassium conductance has the same form as

$$a + b\, e^{-t/\tau_n} + c\, e^{-2t/\tau_n} + d\, e^{-3t/\tau_n} + g\, e^{-4t/\tau_n}$$

which is a noninflected fall to a constant value, a. For repolarization from a highly depolarized state, all terms but the last one become vanishingly small; and the fall is described by a simple exponential, $g\, e^{-4t/\tau_n}$. In this case the time constant for decreasing potassium conductance is $\tau_n/4$. The relationship between the rate of rise and the rate of fall of the potassium conductance in the Hodgkin-Huxley equations thus depends on the exponent in Eq. (6). Larger exponents actually provide a better match for the data on the inflected rise of potassium (Hodgkin and Huxley, 1952d; Cole and Moore, 1960); so the relationship between rates is doubtful, and independent variation of τ_n and τ_n^* in the model is at least partially justified.

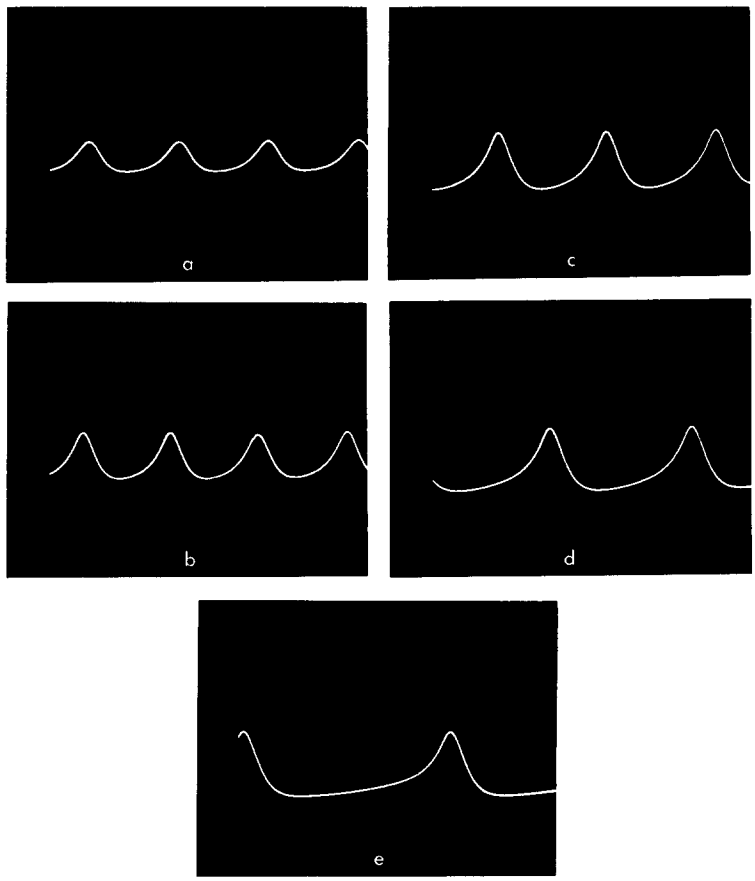

Fig. 18. Periodic oscillations of simulated membrane potential for various magnitudes of τ_n^*, with the simulated membrane capacitance increased by a factor of eight over the value specified by Hodgkin and Huxley. The magnitudes of τ_n^* were as follows: a 5 ms; b 10 ms; c 20 ms; d 40 ms; e 80 ms

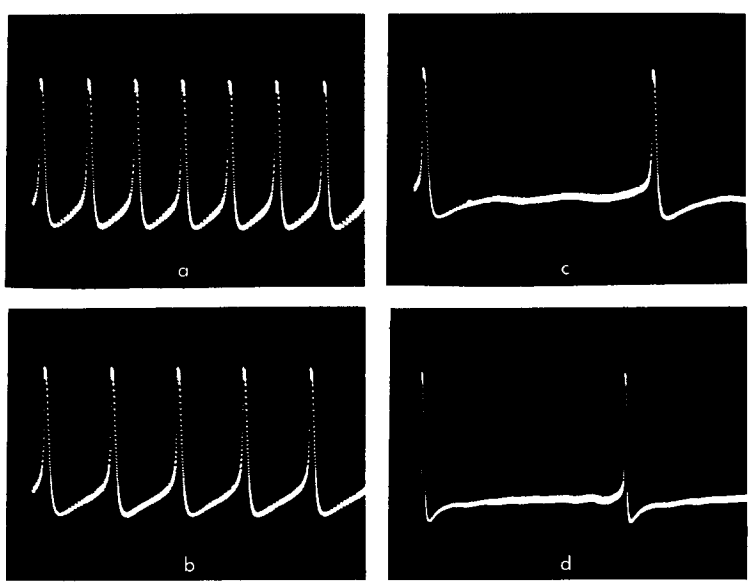

Fig. 19. Periodic spikes for various magnitudes of τ_r. The magnitudes of τ_r were as follows: a 12 ms; b 24 ms; c 50 ms; d 100 ms. The time scale in d was compressed by a factor of two

All of the parameters of the electronic model were adjusted to the values outlined in the table, τ_n being adjusted to 5 ms, the value specified by Hodgkin and Huxley for small excursions of membrane potential.

A steady depolarizing current was applied across the simulated membrane, inducing periodic spikes at a frequency of approximately 40 Hz. The individual spikes were slightly more prolonged than those generated by the model when τ_n was adjusted to its value for large excursions of membrane potential. The time constant (τ_r) of recovery from inactivation of the sodium conductance was increased in three steps from 12 to 100 ms; the effects are shown in Fig. 19. Although the duration of the individual spike was decreased very slightly as τ_r was increased, the over-all appearance of the spike virtually was unchanged. The spike frequency, on the other hand, was changed considerably, decreasing monotonically from 40 to 4 Hz as τ_r was increased from 12 to 100 ms.

With τ_r readjusted to 12 ms, the simulated membrane capacitance was increased to 2 μF, which corresponded to 8 μF/cm² in the squid axon. In this case, the depolarizing current produced periodic subthreshold oscillations instead of spikes. τ_r was increased again from 12 to 100 ms, and the effects are shown in Fig. 20. The frequency of oscillation decreased monotonically with increasing values of τ_r, but the relationship was not linear. The frequency decreased from 10 to 4 Hz, while τ_r was increased from 12 to 100 ms.

Finally, both time constants of sodium inactivation were varied simultaneously. Before each measurement, the voltage-dependent time constant of inactivation (τ_i in the table) and the time constant of recovery from inactivation (τ_r) both were increased or decreased by the same factor from their values specified by HODGKIN and HUXLEY. The factor was varied from measurement to measurement, and the results are shown in Fig. 21. In the case of Fig. 21a, both time constants were one-fourth the magnitudes determined for the squid axon. A steady depolarizing current applied to the model elicited periodic spikes whose amplitudes were approximately 60 per cent that of a full spike in this system. The spike frequency in this case was approximately 40 Hz. In the case of 21b, the time constants were one-half their squid-axon values. The spikes now were nearly full size, but their frequency was still approximately 40 Hz. Fig. 21c shows the periodic spikes when both time constants were equal to their squid-axon values; and 21d through *g* show the effects of increasing these time constants to 2-, 5-, 10- and 20-times the squid-axon values. As these time constants were increased, the spikes became prolonged, exhibiting plateaus; and the spike frequency was diminished. In the case of Fig. 21g, for example, the spike duration was nearly 10 ms and the frequency was approximately 3 Hz.

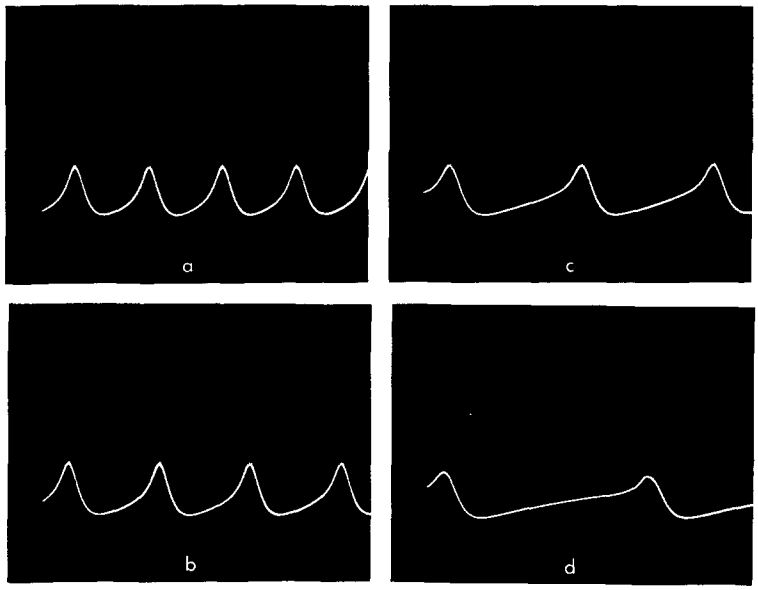

Fig. 20. Periodic oscillations of simulated membrane potential for various magnitudes of τ_r, with the simulated membrane capacitance increased by a factor of eight over the value specified by HODGKIN and HUXLEY. The magnitudes of τ_r were as follows: a 12 ms; b 24 ms; c 50 ms; d 100 ms

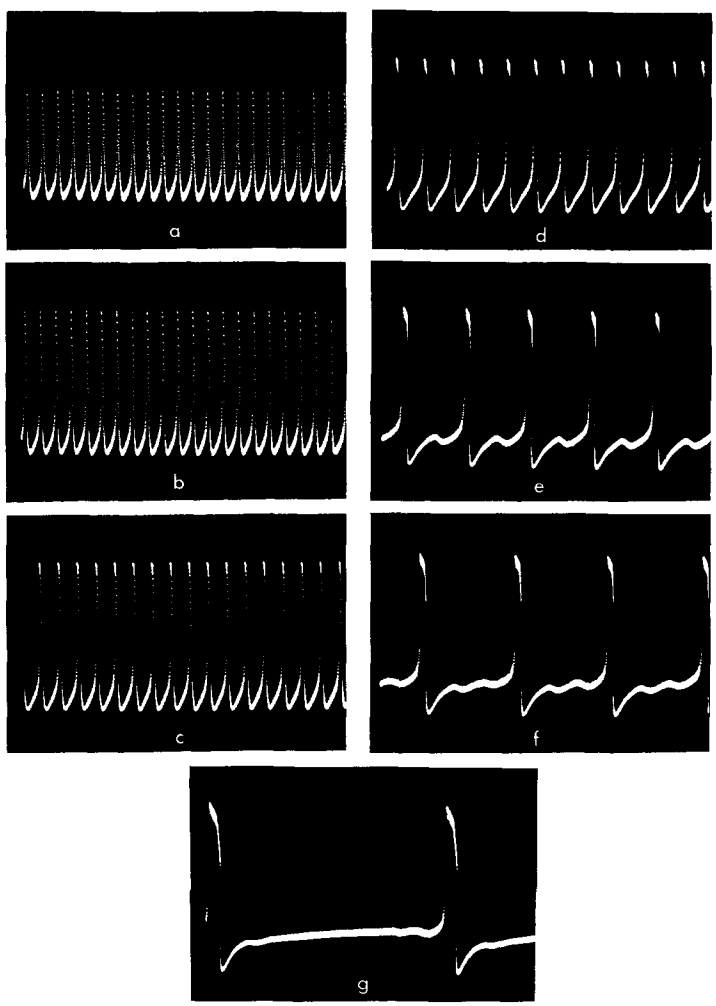

Fig. 21. Periodic spikes for various magnitudes of τ_r and τ_i. See text

The principal effect of increasing the time constant of inactivation was to prolong the spike. This effect is certainly not unexpected, since sodium inactivation is

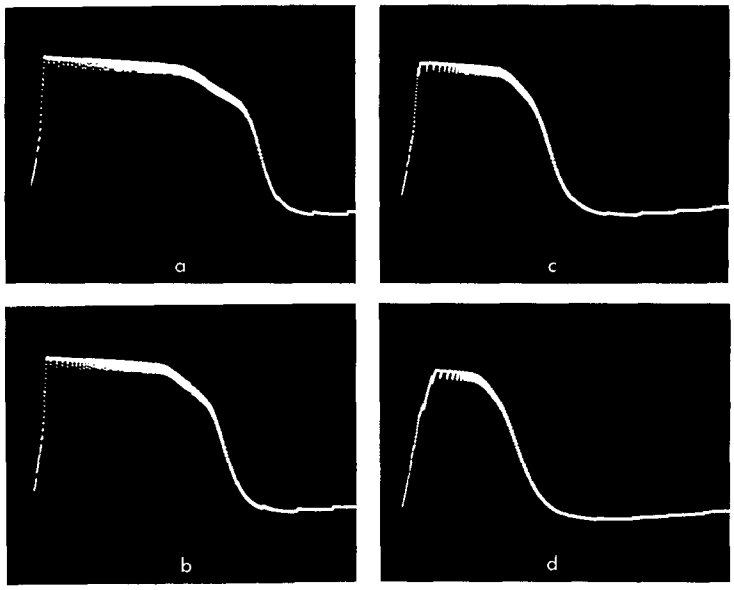

Fig. 22. Periodic plateau potentials in the model, dependence of duration on frequency: a 1 Hz; b 10 Hz; c 20 Hz; d 40 Hz

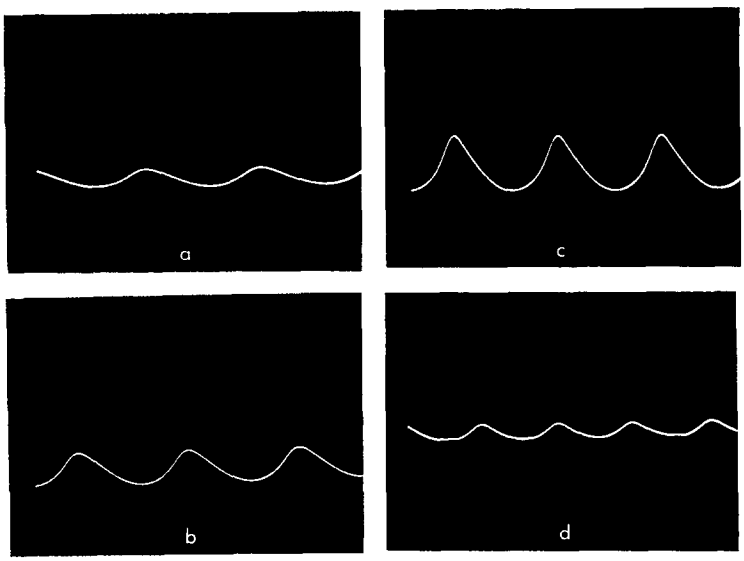

Fig. 23. Periodic oscillations of simulated membrane potential with $\tau_n^* =$ 100 ms and the simulated membrane capacitance twenty times the value specified by HODGKIN and HUXLEY. The *dc* depolarizing current was increased progressively from a to d

an important part of the recovery processes that terminate a spike. When this time constant was decreased to values considerably below its value in the squid axon, on the other hand, the spikes failed to reach their full amplitude. This is simply because the sodium conductance was effectively inactivated before the regenerative depolarization was completed. Increasing the time constant of recovery from inactivation had the opposite effect. The residual inactivation at the time of a spike tended to increase as τ_r was increased. This residue shortened the time required for inactivation and thus tended to shorten the spike duration. The residue also was increased as the spike frequency increased. This effect is evident in the photographs of Fig. 22. In this case the spikes were elicited by a pulse source with controllable frequency rather than by a steady depolarizing current. As the spike frequency was increased, the spike width decreased from approximately 12 ms to approximately 5 ms.

For oscillations in the model that can be classified as subthreshold and graded, the parameters most effective in determining frequency are τ_r and τ_n^*. When τ_n^* and τ_r were adjusted to the values specified by HODGKIN and HUXLEY, the electronic model was unable to sustain oscillations when the simulated membrane capacitance was equivalent to 20 microfarads or more per sq. cm. With increased magnitudes of τ_n^* or τ_r, on the other hand, oscillations could be sustained with higher capacitance values. Fig. 23 shows photographs of oscillations that occurred in the model with τ_n^* equal to 100 ms and C_M equal to 5 μF (equivalent to 20 μF/cm² in the squid axon); all other parameters were adjusted to the values specified in the table. The sequence of photographs shows the effects of increasing the steady depolarizing current that elicited the oscillations. The frequency of oscillation increased monotonically with increasing current, but the amplitude was a nonmonotonic function of current. This particular configuration of the model provided extremely stable, low-amplitude oscillations. The minimum amplitude of stable oscillation in this case was equivalent to less than 5 mV in the squid axon.

With the simulated membrane capacitance equal to 20 μF/cm² and τ_n^* equal to 100 ms, τ_r was increased to 100 ms. Stable low amplitude oscillations again were observed, and the minimum frequency was reduced to 2 Hz. Fig. 24 shows the oscillations in this system and the effects of increasing the steady depolarizing current. Finally, with the simulated membrane capacitance equal to 20 μF/cm² and τ_n^* equal to 100 ms, τ_r and τ_i both were scaled up by the same factors — but with τ_r beginning at 100 ms. In 25b, τ_i was equal to twice the values specified by HODGKIN and HUXLEY; τ_r was 200 ms. In 25c through e, τ_i was scaled to values 5-, 10- and 20-times those in the squid axon, and τ_r was equal to 500 ms, 1 and 2 s respectively. In 25e the frequency of oscillation approaches 1 Hz; but the model no longer bears much resemblance to the squid axon. Its capacitance is twenty times the squid-axon capacitance, and its time constants are 10 to 100 times those of the squid axon.

IV. Conclusions

The electronic model described in this paper was designed for use in a small neural analog facility which recently was completed and which included ten of the models (LEWIS, 1968b). Because ten copies of the model were to be constructed, some approximations and simplifications were incorporated in its design. These approximations and simplifications were made after careful study of an earlier model which did not include most of them (LEWIS, 1964 and 1966). In the

earlier model, τ_m was not neglected; the voltage dependence of τ_n was simulated carefully; a piecewise-linear amplifier was used to match the Hodgkin-Huxley data for n^4; the full range of m^3 was provided; and potentials were neither neglected nor truncated. The model employed copious circuitry including six multipliers; it was not suited for replication. Careful examination of the effects of changing various parameters in this model indicated that its operation was not critically dependent on those parameters mentioned above. Setting τ_m to 0 had no noticeable effect; fixing τ_n at 5 ms led to a slightly prolonged spike with reduced rate of repolarization (LEWIS, 1968b, p.104), but had no noticeable effects on subthreshold phenomena; changing the n^4 characteristics from piecewise linear to linear had no noticeable effect; limiting the range of m^3, particularly for membrane potentials below 6 mV had very little effect; truncating V_{Na}, of course led to truncated spikes; but neglecting the factor $(V_{Na} - V_M)$ had no noticeable effect, provided that I_{Na} approached zero when V_M approached V_{Na}. So the models described in this paper very likely are good realizations of the system they represent.

Individually, the neural models of this paper have been used to examine neuroelectric phenomena available from the combined system of admittances that they represent. Section IIIC illustrates this type of examination. With very minor changes from the parameter settings of the table, the models have provided many of the neuroelectric phenomena observed in living preparations (LEWIS, 1966). They have provided with quantitative fidelity almost all the categories enumerated by BULLOCK (1959) for synaptic responses and spontaneous oscillations. In addition they predicted mutual facilitation by separate excitatory synapses, a phenomenon subsequently observed in the sea hare (KANDEL and TAUC,1 964); and they predicted multimodal distributions of spontaneous-spike intervals, a phenomenon subsequently observed in cat lateral geniculate (BISHOP et al., 1964).

These results are encouraging and tend to support the hypothesis stated at the outset of this paper (i.e., that the Hodgkin-Huxley descriptions of electrically excitable conductances can be combined with the Eccles descriptions of synaptically induced conductances to account for most of the neuroelectric phenomena exhibited by single neurons). An important question generated by this hypothesis is, "what neuroelectric phenomena in single neurons cannot be accounted for by the combined Hodgkin-Huxley-Eccles descriptions without gross perturbations of the latter?"

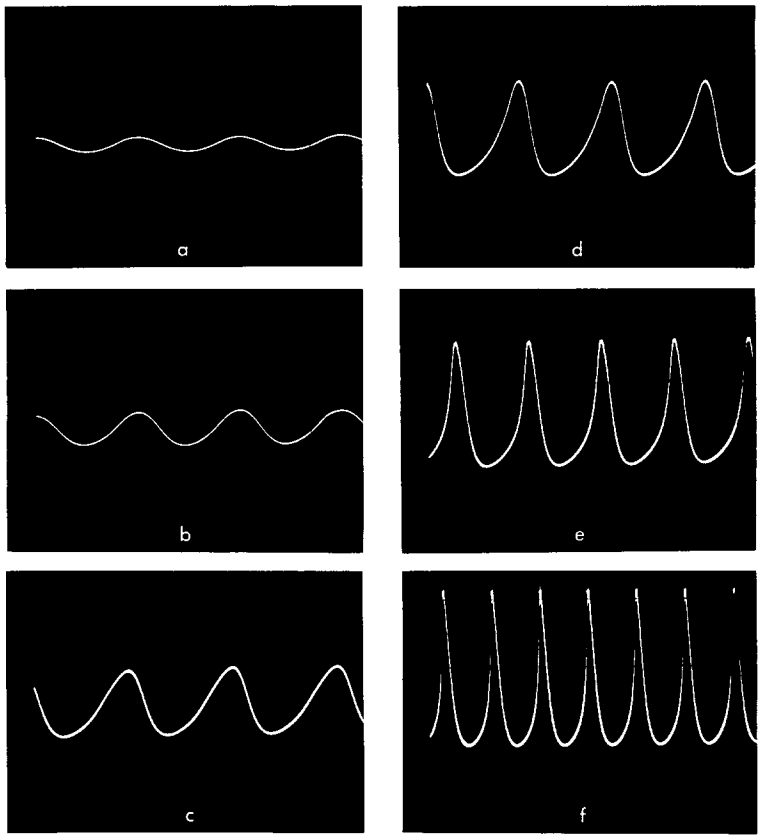

Fig. 24. Periodic oscillations of simulated membrane potential with $\tau_n^* =$ 100 ms, $\tau_r = 100$ ms and the simulated membrane capacitance twenty times the magnitude specified by HODGKIN and HUXLEY. The *dc* depolarizing current was increased progressively from a to f

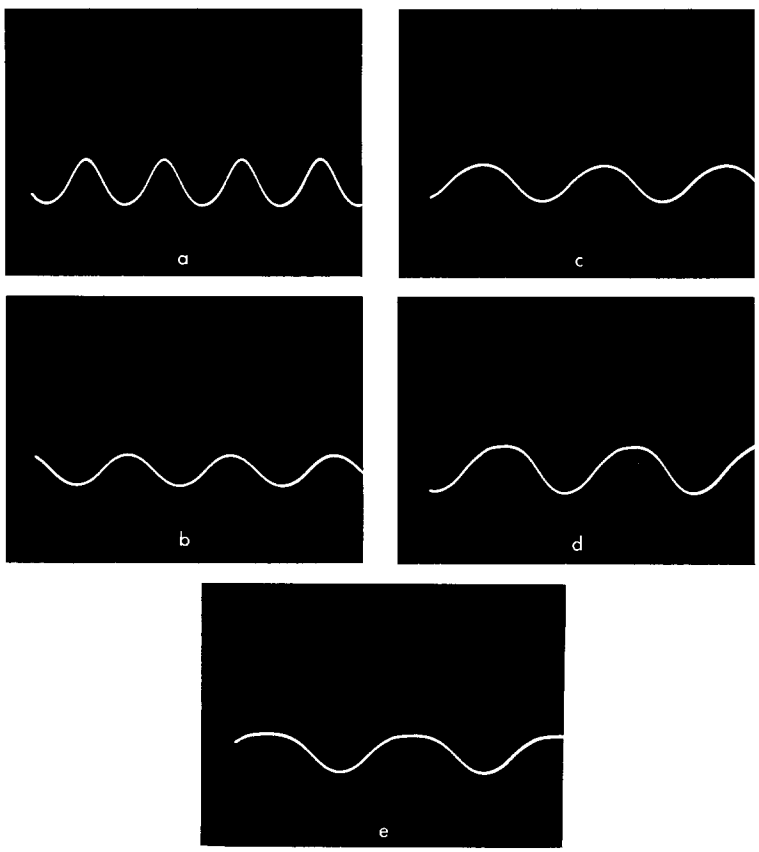

Fig. 25. Periodic oscillations of simulated membrane potential with $\tau_n^* =$ 100 ms, membrane capacitance twenty times the magnitude specified by HODGKIN and HUXLEY, and both time constants of sodium inactivation progressively increased by the same factor. See text

Two such phenomena occur in the lobster cardiac ganglion. Watanabe (1958) has observed 1 Hz subthreshold oscillations in one of the five large neurons of that ganglion. The temperature of the ganglion during his experiments was between 20° C and 25° C. The parameter values in the table were obtained by Hodgkin and Huxley at 6° C. Time constants associated with squid-axon conductances apparently decrease with increasing temperature, so the frequencies of oscillation in the axon at 25° C should be considerably higher than the frequencies at 6° C. Yet according to the results in III C, in order to provide 1-Hz oscillations the electronic model had to be modified until its time constants were 10 to 100 times those specified for the 6°-C squid axon and its capacitance 20 times the squid axon capacitance. 4-Hz oscillations were obtained easily in the model, but 1-Hz oscillations were very difficult to obtain. Another cardiac-ganglion phenomenon that is difficult to explain in terms of the model is that of the *dc* current-voltage characteristics (Hagiwara et al., 1959; Hagiwara, 1960). Several plausible models incorporating the *dc* current-voltage characteristics of the squid axon have failed even to produce characteristics close to those of the cell bodies of the cardiac ganglion (Lewis, 1968b). So our model certainly would seem to be of only limited value in a simulation of the lobster cardiac ganglion.

The ten models of the neural analog facility have been used in several simulation studies. They have been connected by resistors to provide lumped approximations to an axon. They have been connected into pairs to provide two-lump neural models (the simplest configuration that can simulate the interactions between an integrative region of a neuron and a trigger region). And the two-lump models have been combined to simulate small neural networks, including the lobster cardiac ganglion. All of these studies have been reported elsewhere (Lewis, 1968a, b).

As mentioned in the introduction, many of the important problems in neurophysiology are concerned with extremely large neural systems. When one sets out to model these larger systems, the tacit assumption is that the details of neuroelectric point processes become progressively less important as the system becomes larger. The circuit described in this paper may be useful for very small neural networks, but parameter management and size would soon get out of hand if one attempted to extend its use to larger networks. Yet some details of point processes may still be important in these larger nets. Many investigators have offered models that are not nearly as complex as that described in this paper, but which nontheless retain many of the characteristics of neuroelectric point processes (Jenik, 1964; FitzHugh, 1961; Harmon, 1959; Hiltz, 1965; Lewis, 1968a). Those characteristics that are retained in each case represent the modeler's personal hypothesis as to which properties are important in the operations of larger nets. All neural modelers share one common hope: that considerable simplification will be possible as we approach the large central systems with their billions of neurons.

References. Bishop, P. O., W. R. Levick, and W. O. Williams: Statistical analysis of the dark discharge of lateral geniculate neurons. J. Physiol. (Lond.) **170**, 598—612 (1964). — Bullock, T. H.: Neuron doctrine and electrophysiology. Science **129**, 997—1002 (1959). — Cole, K. S., and J. W. Moore: Potassium ion current in the squid giant axon: dynamic characteristic. Biophys. J. **1**, 1—14 (1960). — Eccles, J. C.: The physiology of synapses. Berlin-Göttingen-Heidelberg: Springer 1964. — FitzHugh, R.: Thresholds and plateaus in the Hodgkin-Huxley nerve equation. J. Gen. Physiol. **43**, 867—896 (1960); — Impulses and physiological states in theoretical models of nerve membrane. Biophys. J. **1**, 445—466 (1961). — Frankenhaeuser, B., and A. L. Hodgkin: The after-effects of impulses in the giant fibres of *Loligo*. J. Physiol. (Lond.) **131**, 341—376 (1956). — Hagiwara, S.: Current-voltage relations of nerve cell membrane. In: Electrical activity of single cells, edit. by Y. Katsuki. Tokyo: Igaku Shuin 1960. — Hagiwara, S., A. Watanabe, and N. Saito: Potential changes in syncytial neurons of lobster cardiac ganglion. J. Neurophysiol. **22**, 554—572 (1959). — Harmon, L. D.: Artificial neuron. Science **129**, 962—963 (1959); — Problems in neural modeling. In: Neural theory and modeling, edit. by R. F. Reiss. Stanford: Stanford University Press 1964. — Harmon, L. D., and E. R. Lewis: Neural modeling. Physiol. Rev. **46**, 513—591 (1966). — Hiltz, F. F.: Simulated membrane junctions and additional feedback characteristics for an artificial neuron. IEEE Trans. Bio-Med. Eng. **12**, 94—104 (1965). — Hodgkin, A. L., and A. F. Huxley: Currents carried by sodium and potassium ions through the membrane of the giant axon of *Loligo*. J. Physiol. (Lond.) **116**, 449—472 (1952a); — The components of membrane conductance in the giant axon of *Loligo*. J. Physiol. (Lond.) **116**, 473—496 (1952b); — The dual effect of membrane potential on sodium conductance in the giant axon of *Loligo*. J. Physiol. (Lond.) **116**, 497—506 (1952c); — A quantitative description of membrane current and its application to conduction and excitation in nerve. J. Physiol. (Lond.) **117**, 500—544 (1952d). Hodgkin, A. L., A. F. Huxley, and B. Katz: Measurement of current-voltage relations in the membrane of the giant axon of *Loligo*. J. Physiol. (Lond.) **116**, 424—448 (1952). — Jenik, F.: Pulse processing by neuron models. In: Neural theory and modeling, edit. by R. F. Reiss. Stanford: Stanford University Press 1964. — Kandel, E. R., and L. Tauc: Mechanism of prolonged heterosynaptic facilitation. Nature (Lond.) **202**, 145—147 (1964). — Lewis, E. R.: Neural analog studies. Semi-annual Report, vol. 7, Librascope Division, General Precision, p. 1—58, 1964; — Neuroelectric potentials derived from and extended version of the Hodgkin-Huxley model. J. Theor. Biol. **10**, 125—158 (1966); — Using electronic circuits to model simple neuroelectric interactions. Proc. IEEE **56**, in press (1968a); — Models of neuroelectric interactions. Wright-Patterson Air Force Base, Ohio, Aerospace Medical Research Laboratories, 1968b. — Rall, W.: Theoretical significance of dendritic trees for neuronal input-output relations. In: Neural theory and modeling, edit. by R. F. Reiss. Stanford: Stanford University Press 1964. — Watanabe, A.: The interaction of electrical activity among neurons of lobster cardiac ganglion. Jap. J. Physiol. 8, 305—318 (1958).

Prof. Dr. E. R. Lewis
Department of Electrical Engineering
and Computer Sciences and the
Electronics Research Laboratory
University of California
Berkeley, California, U.S.A.

Verantwortlich für den Textteil: Prof. Dr. W. Reichardt, 7400 Tübingen, Max-Planck-Institut für Biologie, Spemannstr. 38 — Verantwortlich für den Anzeigenteil: Edgar Seidler, 1 Berlin 33, Heidelberger Platz 3. — Springer-Verlag, Berlin · Heidelberg · New York. — Druck der Universitätsdruckerei H. Stürtz AG., Würzburg. — Printed in Germany